Environment International 198 (2025) 109440

Contents lists available at ScienceDirect

Environment International

journal homepage: www.elsevier.com/locate/envint

Full length article

In vitro genotoxic and mutagenic potentials of combustion particles from marine fuels with different sulfur contents

Seongho Jeong [a,b], Jana Pantzke [a,b], Svenja Offer [a,b], Uwe Käfer [a,b], Jan Bendl [c], Mohammad Saraji-Bozorgzad [c], Anja Huber [a,b], Bernhard Michalke [d], Uwe Etzien [e], Gert Jakobi [a], Jürgen Orasche [a], Hendryk Czech [a,b], Christopher P. Rüger [b,f], Jürgen Schnelle-Kreis [a], Thorsten Streibel [a,b], Bert Buchholz [e], Thomas Adam [a,c], Martin Sklorz [a,b], Sebastiano Di Bucchianico [a,b,f,*], Ralf Zimmermann [a,b,f]

[a] Comprehensive Molecular Analytics, Helmholtz Zentrum München, Ingolstädter Landstr. 1, 85764 Neuherberg, Germany
[b] Chair of Analytical Chemistry, Institute of Chemistry, University of Rostock, Albert-Einstein-Strasse 27, 18059 Rostock, Germany
[c] University of the Bundeswehr Munich, Faculty for Mechanical Engineering, Institute of Chemistry and Environmental Engineering, Werner-Heisenberg-Weg 39, 85577 Neubiberg, Germany
[d] Research Unit Analytical BioGeoChemistry, Helmholtz Zentrum München, Ingolstädter Landstr. 1, 85764 Neuherberg, Germany
[e] Chair of Piston Machines and Internal Combustion Engines, Faculty of Mechanical Engineering and Marine Technology, University of Rostock, Albert-Einstein-Strasse 2, 18059 Rostock, Germany
[f] Department Life, Light & Matter, University of Rostock, Albert-Einstein Strasse 25, 18059 Rostock, Germany

ARTICLE INFO

Handling Editor: Marti Nadal

Keywords:
Marine Gas Oil (MGO)
Heavy Fuel Oil (HFO)
Particulate Matter (PM)
Ship emission
Genotoxicity
Mutagenicity

ABSTRACT

Ship emissions significantly impact both the environment and human health. To address these concerns, the International Maritime Organization has imposed restrictions on the sulfur content in marine fuels. Specifically, the fuel sulfur content (FSC) must be below 0.5% m/m globally and below 0.1% m/m in designated sulfur emission control areas. These regulations apply to a range of fuels including distillate diesel-like fuels and low-sulfur heavy fuel oils (HFOs). As a result, there has been a reduction in emissions, particularly sulfur oxides and particulate matter (PM). However, the relationship between FSC and the toxicity of ship emissions remains unclear. This study aimed to investigate how the physical and chemical properties of PM from a marine engine operating on five marine fuels with varying FSCs, influence toxicological outcomes. For this scope, the study assessed cytotoxic, genotoxic, mutagenic, and pro-inflammatory effects of the emitted particles using lung cell models. The involvement of intracellular reactive oxygen species and xenobiotic metabolism was also examinated. The results showed that PM from the combustion of different fuels reduced cell viability and clonogenicity at the highest concentration. However, other toxicological outcomes, such as genotoxic potential, were more strongly associated with the polycyclic aromatic hydrocarbon content of the PM than with FSC. Notably, an aromatic-rich HFO with intermediate FSC induced a significant increase in gene mutation frequency and alterations of cellular processes. In conclusion, while reducing FSC is an important step in mitigating ship emissions, this study underscores the need for a comprehensive evaluation of fuel properties.

1. Introduction

Deteriorating air quality, characterized by elevated concentrations of airborne particulate matter (PM) from anthropogenic sources such as combustion processes, poses a significant threat to human health. Inhalation of these pollutants can trigger oxidative stress and inflammation, which are associated with the onset of cardiovascular and respiratory diseases. These conditions contribute to increased mortality rates from cardiopulmonary diseases and lung cancer (Vilas-Boas et al., 2024). While stringent regulations and advanced flue gas aftertreatment technologies, such as particle filters and oxidation catalysts, have significantly reduced emissions from land-based vehicles (Eyring et al., 2005; Ramacher et al., 2020), ship emissions remain a pressing concern. This is largely due to less stringent regulations and the limited

* Corresponding author at: Department Life, Light & Matter, University of Rostock, Albert-Einstein Strasse 25, 18059 Rostock, Germany
E-mail address: s.dibucchianico@uni-rostock.de (S. Di Bucchianico).

https://doi.org/10.1016/j.envint.2025.109440
Received 24 January 2025; Received in revised form 27 March 2025; Accepted 4 April 2025
Available online 10 April 2025

adoption of emission abatement systems in the marine sector. For example, the sulfur content allowed in marine fuels is substantially higher than that permitted in fuels for land-based vehicles. This discrepancy leads to significantly higher emissions per unit of fuel consumed, particularly for PM and sulfur oxides (SO_x) (Moldanová et al., 2013; Huang et al., 2018). Additionally, these pollutants not only increase primary PM concentrations but also act as precursors for the formation of secondary PM in the atmosphere. Consequently, ship emissions are recognized as significant contributors to adverse health outcomes, including morbidity and premature mortality, especially in region near harbors and coastal cities (Corbett et al., 2007; Fuglestvedt et al., 2009; Hong et al., 2023).

To address the issue of ship emissions, the International Maritime Organization (IMO) introduced a series of guidelines aimed at reducing fuel sulfur content (FSC) to 0.1 % m/m in designated sulfur emission control areas (SECAs) and 0.5 % outside of SECAs (IMO, 2008). Compliance can be achieved by using low-sulfur fuels, such as marine gas oil (MGO), low-sulfur heavy fuel oil (HFO), or hybrid fuels. Alternatively, the use of high-sulfur HFOs is allowed if emission reduction technologies, such as scrubbers, are installed to achieve sulfur emission levels comparable to those of low-sulfur fuels. Epidemiological and modeling studies suggest that stricter SECA regulations and the transition to low-sulfur fuels could lead to significant reductions in pollutants such as $PM_{2.5}$, sulfates, metals, and SO_x (Repka et al., 2021; Jang et al., 2023). This would, in turn, reduce morbidity and mortality rates associated with air pollution (Sofiev et al., 2018). Experimental studies further show that replacing conventional low-grade HFO with high-quality distillate fuels results in significant decreases in both the number and mass of particle emissions (Moldanová et al., 2013; Kuittinen et al., 2021). Other research highlights the influence of engine operation conditions on particulate emissions, with reduced emissions observed during optimized operations such as open-sea cruising, compared to higher emissions during maneuvering phases (Sippula et al., 2014; Mueller et al., 2015; Streibel et al., 2017). Despite these advancements, the environmental impacts of the physical and chemical characteristics of PM constituents derived from various fuel types and their associated toxicological potentials remain poorly understood. Further investigation into these aspects is critical to fully address the healthy and environmental risks of ship emissions. Bauer et al. (2024) recently demonstrated that FSC does not always determine the composition of PM, particularly for global SECA-compliant fuels. Similarly, Anders et al. (2024) found that even MGO emissions contain particles with distinct signatures of polycyclic aromatic hydrocarbons (PAHs), such as phenanthrene and its alkylated derivatives. Jeong et al. (2023) observed only a minor reduction in particle number and mass emission factors when using a sulfur scrubber that complies with current IMO regulations, emphasizing the need for additional abatement systems to further reduce particulate emissions. Bendl et al. (2024) investigated gaseous emission from various marine fuel types, revealing that switching fuel types can reduce certain toxic gas emissions, such as formaldehyde and acetaldehyde. However, other emissions, like Benzene from low-sulfur HFO, remained unchanged even with after-treatment systems. Rosewig et al. (2024) provided real-world detection of ship-emission particles detected at a harbor, showing that ships with sulfur scrubbers still emit PM containing transition metals, such as Iron, Nickel, and Vanadium. These metals are known to originate from heavy fuel oil combustion (Celo et al., 2015). These findings suggest that merely reducing FSC in marine fuels is insufficient to significantly mitigate the environmental burden of ship emissions. This is true not only for direct emission but also for their role as precursors in secondary aerosol formation (Aksoyoglu et al., 2016). Beyond environmental impacts, studies on the toxicological potential of particulate emissions from different marine fuels reveal concerning health risks. For instance, Wu et al. (2018) reported that PM from HFO combustion induces acute toxicity, causing higher cytotoxicity and oxidative stress in human lung epithelial cells compared to diesel-like fuels. However, this does not imply that diesel-like fuel PM lacks health relevance. Oeder et al. (2015) and Sapcariu et al. (2016) found that PM from diesel-like fuels elicited a broader range of responses in human lung cells. These emissions more strongly influenced critical pathways of cell metabolism, including energy metabolism, protein synthesis, and chromatin modification, demonstrating their potential to affect cellular function extensively. These findings highlight the need to consider the specific characteristics of emissions from different marine fuel types when evaluating the effectiveness of FSC reductions. They also emphasize the importance of further investigation into the environmental and health impacts of these emissions. With the anticipated growth of global trade and international supply chains, expected to increase shipping emissions, there is an urgent need for research to assess the differential toxicological potential of emitted pollutants and guide mitigation strategies. While previous studies have evaluated PM from individual fuels or focused on toxicological potentials, the present work integrates multiple endpoints, including genotoxic as well as mutagenic potentials, under controlled experimental conditions, allowing direct comparison between fuel types. To the best of the authors' knowledge, no prior study has investigated the effects of PM from the combustion of five distinct marine fuels, including MGO and HFOs on mammalian cells. By integrating fuel specific emission profiles with a wide range of biological endpoints, the current work provides a deeper understanding of complex relationship between combustion-derived PM composition and biological effects. In particular, this study offers a comprehensive *in vitro* assessment, uniquely addressing the impacts of fine PM ($PM_{2.5}$) from ship emissions by considering both physical and chemical variations, such as differences in FSC and aromaticity, given that fine PM is known to penetrate deeply into the respiratory system and deposit in lung tissues (Cipoli et al., 2023). The aim of this study is to evaluate the toxicological effects of PM from five different marine fuels, spanning an FSC range from 0.06 % m/m to 2.4 % on lung cells, under varying concentrations and exposure durations. The analysis includes assessments of cytotoxicity, clonogenicity, genotoxicity, and mutagenicity, as well as the ability of emitted particles to induce oxidative stress, xenobiotic metabolism, and pro-inflammatory responses. These effects are examined in relation to physical and chemical parameters, such as particle number size distribution, particle mass emission factors, organic composition, and metal contents. By providing a detailed evaluation of the toxicological effects associated with ship emissions, this study aims to deepen our understanding of their health-related impacts. The findings are expected to inform policy development and support the implementation of mitigation strategies in the shipping industry.

2. Material and Methods

2.1. Characterization of the ship engine and marine fuel types

In order to mimic realistic combustion processes of a marine engine with a stable and reproducible emission scenario, a four-stroke, single-cylinder, common rail research marine engine at the University of Rostock was used. The engine, with a rated power of 80 kW at 1500 rpm, was designed as a representative of a typical modern medium-speed marine engine and was equipped with a compressor-charged air-intake for fixable air–fuel equivalence ratios. Further detailed specifications of the test engine can be found in previous studies (Mueller et al., 2015; Streibel et al., 2017). The engine was operated on fixed cycles at four different engine loads of 20, 40, 60, and 80 kW for each fuel type, corresponding to 25, 50, 75, and 100 % of the maximum continuous rate, respectively. The duration and sequence of the engine loads were determined according to the weighting factors of ISO 8178–4 E2, with a total cycle duration of 6 h. Specifically, the engine loads of 20 kW and 40 kW were maintained for 54 min, 60 kW for 180 min, and 80 kW for 72 min. It is noteworthy that the entire test cycle was repeated three times with each fuel type, followed by an exchange of the lubricating oil for the subsequent test cycle with a different fuel type.

Five different marine fuels were utilized in the present study,

comprising one MGO and four HFOs. MGO is regarded as one of the highest quality marine fuels due to its low sulfur and metal contents compared with HFO. In contrast, HFOs generally exhibit higher viscosity and density, and often contain residual fractions resulting from refinery processes (Fritt-Rasmussen et al., 2018). Consequently, HFOs can contain substantial quantities of metals (predominantly Ni, V, and Fe), sulfur, and nitrogen. By definition, an HFO has a density greater than 0.9 g cm^{-3} at 15 °C or a kinematic viscosity exceeding 180 mm^2 s^{-1} at 50 °C (Fritt-Rasmussen et al., 2018), allowing for a broad range of marine fuels to be produced through the blending of different product streams from the crude oil refining. For the purpose of this study, MGO, low-sulfur HFO (LS-HFO), and high-sulfur HFO (HS-HFO) were purchased as commercial marine fuels. In addition, two blended non-commercial fuels, an ultra-low sulfur HFO (ULS-HFO_{AR}) and a high sulfur HFO (HS-HFO_{SYN}), containing high amounts of aromatic compounds were investigated. Despite the fact that the FSC is associated with the high-boiling fractions of HFOs (Hsieh et al., 2013), LS-HFO demonstrated the least mass loss in boiling distribution analysis up to 400 °C (Fig. S1). ULS-HFO_{AR} has been found to demonstrate a high degree of similarity to distillate fuels, such as MGO with regard to sulfur and metal contents, viscosity, and flash point, despite its categorization as an HFO and its low combustion efficiency. This fuel type is divided from to a clarified cycle oil, which is produced through the process of fluid catalytic cracking, and is predominantly composed of alkylated 2- to 4-ring aromatics (Käfer et al., 2019). HS-HFO_{SYN} features typical properties of HFO but comprises distinct low- and high-boiling fractions in a ratio of approximately 30:70. The combustion efficiency of each fuel type is expressed in Table 1 as C/H ratio (m/m), calculated carbon aromaticity index (CCAI), and aromaticity index (AI) (Koch and Dittmar, 2016). The highest C/H, CCAI, and AI values of ULS-HFO_{AR} resulted in the lowest ignition quality, which led to a maximum engine load of 68 kW instead of 80 kW.

2.2. Sampling setup and particle collection

The configuration of the collection and characterization of particles is illustrated in Fig. 1. Particle emissions from the engine exhaust were collected using two different dilution systems: one for toxicological assessment and chemical characterization (offline) and the other for online particle physical characterization. To prevent vapor condensation on the particle emissions, a 250 °C heat transfer line was installed between the sampling point and dilution system for both sampling lines of offline and online instruments. The dilution system (Venacontra, Finland) utilized for the toxicology study comprised a porous tube diluter (PTD). The particles were subsequently directed into an ejector diluter (EJD), which thoroughly mixed the sample with the dilution air. The dilution factor was set between 5 and 10, depending on the FSC and its dew point at 25 °C, in order to inhibit the condensation of sulfuric acid in the dilution system while ensuring maximum particle yield. The precise dilution factor was calculated by utilizing a CO_2 probe (GMP 343, Vaisala, Finland) to calculate the CO_2 concentration and compare it with the raw gas and background CO_2 concentration in the dilution air, as previously described by Grigonyte et al. (2014). The separation of coarse particles (PM_{10}), from the exhaust emissions was performed using a pre-cyclone, and particles smaller than PM_{10} were collected in a commercially available sampling box (CGS GmbH, Germany). A ceramic filter (1011756, CGS GmbH, Germany) was utilized to collect particles directly on the filter surface. The particles were sampled with a volume flow of 50 L min^{-1} after appropriate dilution and cooling to 25 °C. Subsequent to the measurement cycle, the particles collected on the ceramic filter were carefully scratched off using a sterile stainless spatula and stored in a sterile glass vial at −20 °C. In order to avoid any possible interruptions to the online equipment, a separate sampling point was configured for the purpose of particle characterization. The exhaust was diluted using a two-stage EJD system (eDiluter, Dekati Ltd., Finland). The dilution ratio of the eDiluter was optimized based on the detection limits of the online equipment, with the dilution factor adjusted between 25 and 100, depending on the particle number concentration of different fuel types. To further enhance the precision of the measurement, additional dilution steps were implemented using EJDs (VKL 10, Palas GmbH, Germany) with a fixed dilution factor of 10.

Table 1
Physical and chemical properties of applied fuels.

	Method	MGO	ULS-HFO_{AR}	LS-HFO	HS-HFO_{SYN}	HS-HFO
Density at 15 °C [g/cm^3]	ISO 12,185	0.835	0.975	0.96	1.01	0.990
Viscosity at 50 °C [mm^2/s]	ISO 3104	2	6	340	380	350
Sulfur [% m/m]	DIN 51400–10	0.001	0.048	0.51	1.02	2.16
Water [mg/kg]	ISO 12,937	23	214	423	1030	586
Flash point [°C]	ISO 2719	72	75	156	147	135
Ash [% m/m]	ISO 6254	0.001	< 0.001	0.019	0.019	0.051
Heating value [MJ/kg]	DIN 51900–1,3	42.7	40.3	41.1	40.1	40.1
C/H [-]	DIN 51,732	6.9	10.3	7.8	9.2	8.6
CCAI [-]	ISO 8217	796	907.4	822	871	852
AI [-]	Calculated*	0.27	0.55	0.37	0.49	0.44
Ni [mg/kg]	ICP-MS	< 1	< 1	19	38	61
V [mg/kg]	ICP-MS	< 1	2	25	57	240
Fe [mg/kg]	ICP-MS	< 1	< 1	11	26	52

*Calculated according to Koch and Dittmar (2016).

2.3. Physical and chemical characterization of particles

Particles emitted from each complete test cycle were collected separately for analysis of their physical and chemical properties within three experiments. Due to the limited amount of PM sampled, only one elemental analysis was performed for each HFO PM, while no measurements could be performed for the MGO PM.

2.3.1. Online physical characterization

A comprehensive study of the particle size distribution, number, and mass concentrations was performed using a scanning mobility particle sizer (SMPS) and a tapered element oscillating microbalance (TEOM 1400a, Thermo Fisher Scientific, USA). The SMPS operated at an aerosol flow rate of 0.3 L min^{-1}, equipped with an X-ray neutralizer (TSI, Model 3088, USA), an electrostatic classifier (TSI, Model 3082, USA), and a condensation particle counter (TSI, Model 3750, USA). The TEOM measured the particle mass concentrations at a sample flow rate of 3 L min^{-1}, with a cap and inlet tube temperature of 50 °C, as per the standard settings described by Patashnick and Rupprecht (1991). To account for potential artifacts in gaseous and particulate emissions during engine load transitions, only measurements taken after a stabilization period of approximately 30 min were considered valid. Additionally, an aethalometer (AE33-7, Magee Scientific, Aerosol, d.o.o., Slovenia) was employed for real-time monitoring of the light absorption properties of PM to ascertain the equivalent mass concentration of black carbon (eBC).

2.3.2. Polycyclic aromatic hydrocarbons (PAHs)

The quantification of PM-bound PAHs was achieved through the analysis of collected PM using direct thermal desorption comprehensive two-dimensional gas chromatography coupled to high-resolution time-of-flight mass spectrometry (DTD-GC × GC-HRTOFMS). The applied analytical method is based on previous studies (Schnelle-Kreis et al., 2005; Orasche et al., 2011) and adapted for the application on a Leco

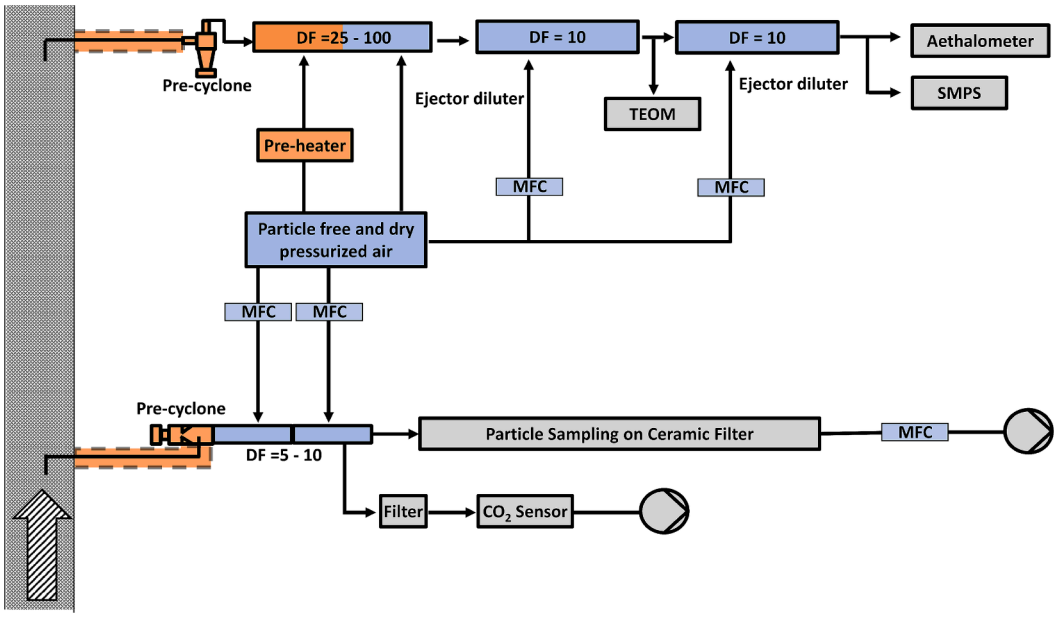

Fig. 1. Scheme for the sampling setup. The arrow with stripe pattern indicates the ship emission from the engine. TEOM, tapered element oscillating microbalance; SMPS, scanning mobility particle sizer; DF, dilution factor; MFC, mass flow controller.

Pegasus HRT 4D system (Leco, USA) with an Optic 4 programmable vaporizing injector (GL Science, the Netherlands). Defined aliquots of approximately 1 mg of particles were homogenized with baked out, grounded sodium sulfate (1:1,000, w/w), which served as inert matrix for dilution. This approach facilitates subsequent sample handling steps and prevents overloading of the analytical setup. From these mixtures, precisely weighted amounts in the range between 20 and 40 mg were transferred to a GC-liner and spiked with an internal standard mixture, containing deuterated PAHs. Subsequently, the prepared samples were analyzed using DTD-GC × GC-HRTOFMS with three repetitions for each sample. Detailed information about thermal desorption, chromatographic, and mass spectrometric parameters can be found in Table S1. Quantification of the 12 target PAHs was performed by internal standard correction and external calibration with the same approach as previously described by Schnelle-Kreis et al. (2005) and Orasche et al. (2011).

2.3.3. PM elemental content measured by ICP-OES

Elemental analysis was performed on collected PM, which was suspended in 1 mL of sub-boiling distilled 65 % nitric acid (Roth, Germany) overnight and subsequently diluted with 3 mL of Milli-Q water. The resulting PM suspension was filtered using one-way syringe filters (0.22 μm, VWR, Germany) and then analyzed using inductively coupled plasma atomic emission spectroscopy (ICP-OES, ARCOS, Germany). The resulting data are expressed in μg mg^{-1} of particle mass, and the limit of quantification is delineated in Table S3. To determine the measurement uncertainty (*Unc)* for each element *(i),* equation 1 was employed:

$$Unc(i) = \left[(analyteconcentration(i) \times instrumentprecision)^2 + LOD^2 \right]^{1/2} \quad (1)$$

with LOD being the limit of detection. The LOD term reflects the baseline measurement noise, while the precision term accounts for concentration-dependent variability, providing a comprehensive and robust estimate of measurement uncertainty. In this study, the LOD is calculated according to LOD = $\bar{x}$ + (3*s) ($\bar{x}$: mean of the blank measurements, s: standard deviation of the blank measurements).

2.3.4. Mutagenic equivalent values (BaPMEQ)

The measured PAH concentrations were utilized to calculate the mutagenic potential of PM-bound PAHs by normalizing the mutagenic potential of each PAH to that of Benzo[a]pyrene (BaP). The mutagenic equivalent values (BaPMEQ, ng m^{-3}) of the sampled PM were determined by multiplying the Mutagenic Equivalent Factor (MEF) for each PAH, as reported by Durant et al. (1996) (Table S2), by its corresponding concentration.

2.3.5. PM suspension preparation

In order to prepare PM suspensions for *in vitro* testing, 0.05 % w/v bovine serum albumin (BSA, CAS-9048–46-8, Fraction V, BioMol GmbH, Germany) water solutions were freshly prepared and subsequently diluted in cell culture medium. A 1 % w/v solution of the BSA powder in ultrapure water was prepared, filtered using a sterile syringe filter with a pore size of 0.22 μm (16532-GUK, Sartorius, Germany), and further diluted to a concentration of 0.05 % w/v in ultrapure water. Each type of PM was weighted using a microbalance (MC-1 AC210S, Sartorius, Germany) and aliquoted in a sterile glass vial (548–0509, VWR, Germany). As a prewetting procedure, 0.5 % v/v of ethanol (Panreac AppliChem, Germany) was added to each PM sample in the glass vial. Following a one-minute of the prewetting, the PM was suspended in 0.05 % w/v BSA-water, reaching a concentration of 2 mg mL^{-1}. The suspension was then subjected to sonication (PALSONIC, ALLPAX, Germany) for a duration of 30 min in an icy water bath to prevent excessive heating. During this sonication, the sample was subjected to agitation and stirring at a frequency of once every five minutes. The resulting PM suspensions were then diluted with high-glucose Dulbecco's Modified Eagle Medium/Nutrient Mixture F-12 (CAS 31331–028, DMEM/F12, Gibco) to reach a PM concentration of 1 mg mL^{-1} and sonicated for an additional 5 min. After the second sonication step, the stock solutions were further diluted in cell culture medium to achieve the desired PM concentrations.

2.3.6. Physical characterization of PM suspension

To understand the comprehensive physical characteristics of the PM in the exposure medium for the submerged experiments, the hydrodynamic particle diameter, the polydispersity index (PDI), and the zeta potential were measured. A well-dispersed PM suspension with a concentration of 50 μg mL^{-1} was freshly prepared for the PM from each type of fuel. The hydrodynamic size and PDI were measured using a micro cuvette (ZEN0040, Malvern Instrument Ltd., UK) at room temperature, with a backscatter angle of 173° (Nano ZSP, Malvern Instrument Ltd.,

UK). To measure the zeta potential of PM in DMEM/F12 cell culture media, the PM suspension was added to a folded capillary zeta cell (DTS1070, Malvern Instrument Ltd., UK). Each physical parameter was measured ten times after a 120-second equilibration period for each sample.

2.4. Cell culture and treatments

A549 human alveolar epithelial cells (CCL-185, ATCC®, USA) were routinely cultured and maintained in DMEM/F12 medium supplemented with 5 % v/v heat-inactivated fetal bovine serum (FBS, 10500–064, Thermo Fisher Scientific, USA), 100 U mL^{-1} penicillin, and 100 μg mL^{-1} streptomycin (P4333, Sigma-Aldrich, USA) in a humidified incubator at 37 °C and 5 % CO_2. For the exposure experiments, A549 cells (passages from 5 to 25) were seeded at a concentration of 7.6×10^4 cells cm^{-2} on 24-well plates (Corning®, USA). Following a 24-hour incubation period, PM dispersions were added to the cell cultures, reaching final concentrations of 3.5, 15, and 55 μg cm^{-2} corresponding to 6.25, 25, and 100 μg/mL respectively. The cells were then subjected to further incubation for 4 or 24 h.

2.5. Toxicological responses

In general, cells cultured in cell culture medium DMEM/F12 were designated as negative controls, while cells treated with 0.05 % w/v BSA-water in DMEM/F12 media served as solvent control in all assays.

2.5.1. Cell viability

Cell viability was evaluated using the trypan blue exclusion assay. Following a 4- or 24-hour exposure period, A549 cells were washed twice with prewarmed phosphate-buffered saline (PBS). Thereafter, the cells were detached using 0.05 % trypsin–EDTA (T4174, Sigma-Aldrich, USA). Subsequently, 20 μL of the cell suspension was mixed with an equal volume of 0.4 % w/v trypan blue solution (T8154-20ML, Sigma-Aldrich, USA), and the percentage of viable (unstained) cells was determined using a hemocytometer (Neubauer, Germany).

2.5.2. Colony forming efficiency

Cell proliferation was investigated by measuring the ability of single cells to form a colony consisting of at least 50 cells, referred to as clonogenicity at a given time point, which is closely related to cytotoxicity (Franken et al., 2006; Galluzzi et al., 2012). After 4 and 24 h of exposure, the cells were harvested by trypsinization, counted, and diluted in DMEM/F12 medium with 5 % FBS. A total of 250 cells per well were seeded into 6-well plates (Corning®, USA), and the medium was freshly replaced every two days. After eight days, the formed cell colonies were fixed in PBS for 30 min using 3.4 % v/v formaldehyde (4980.1, Carl Roth, Germany) and stained with 10 % v/v of Giemsa solution (GS500, Sigma-Aldrich, USA) in Milli-Q water for 60 min. Representative images were obtained using the Lionheart FX automated microscope (BioTek, USA), and the colonies were counted employing ImageJ (Fiji, version 1.53c). The results are expressed as the percentage of colony forming efficiency (% CFE) according to equation 2 (Ponti et al., 2014).

$$\%\,\mathrm{CFE} = \left(\frac{\text{Average of number of colonies in treatment}}{\text{Average of number of colonies in the control}}\right) \times 100 \quad (2)$$

2.5.3. DNA damage

In order to assess PM-induced DNA single- and double-strand breaks, the alkaline single-cell gel electrophoresis technique was performed according to the minigel comet assay method as demonstrated in a previous study (Di Bucchianico et al., 2017). Following the designated exposure time, the cells were detached using trypsin, and the cell suspension was subsequently diluted to a concentration of 2,500 cells mL^{-1}. Each sample was then mixed with 1 % of low-melting-point agarose at 37 °C, followed by embedding in a micro-agarose gel in microscope slides (2951–001, Thermo Fisher Scientific, USA). In this study, eight microgels per slide were arranged with untreated controls and PM-exposed cells, as well as a positive control, which was prepared by exposing cells to 30 μM hydrogen peroxide (H_2O_2) on ice for 5 min. Subsequently, the cells within the microgels were lysed in a buffer (2.5 M NaCl, 0.1 M EDTA, 10 mM Tris, and 1 % Triton X-100, pH 10) in the dark on ice for an hour. To unwind the nuclear DNA, the slides were immersed in an alkaline electrophoresis buffer (300 mM NaOH, 1 mM EDTA, pH > 13) in the dark on ice for 30 min. Under an electric field generated by electrophoresis, the migration of damaged DNA toward the anode was achieved at 25 V with a current of 300 mA for 20 min. Then, each slide was rinsed with cold 0.4 M Tris (A411.1, Carl Roth, Germany) for 10 min, followed by rinsing with cold water for an additional 10 min, and left for drying at least overnight. The DNA was stained with a 1:10,000 diluted SYBR Green (S11494, Thermo Fisher Scientific, USA) in TE (Tris–EDTA) buffer (10 mM Tris–HCl, 1 mM EDTA, pH 7.5). Images were obtained using a Lionheart FX automated microscope to obtain micrographs at 20-fold magnification. The analysis of one hundred nucleoids per minigel was conducted using CometScore 2.0 software (TriTek Corp., USA), and the results are presented as the mean percentage of DNA in the tail, with standard error of the mean calculated from three independent exposures.

2.5.4. Intracellular reactive oxygen species

The 2,7-dichlorodihydrofluorescein diacetate (H_2DCF-DA) assay was utilized to investigate the potential of PM to induce oxidative stress. For the intracellular ROS assay, A549 cells were seeded in 96-well plates at a density of 4×10^4 cells cm^{-2} 24 h before exposure. The cells were preloaded with 100 μL of 20 μM H_2DCF-DA in HBSS (with Ca^{2+} and Mg^{2+}) for 30 min in a CO_2 incubator at 37 °C, followed by twice washing with prewarmed HBSS. Subsequently, the cells were then exposed to the PM suspension in DMEM (31053, Thermo Fisher Scientific, USA) without phenol red to avoid possible interference. A positive control was established using 25 μM *tert*-butyl hydroperoxide (8.14006, Sigma-Aldrich, USA) in HBSS. Subsequent to the exposure to PM, the kinetic fluorescence was measured to quantify the increase of the fluorescence intensity, with an excitation/emission wavelength of 485/535 nm in a microplate reader at 37 °C (Varioskan™ Lux, Thermo Fisher Scientific, USA) for a period of 4 h. The detected ROS levels were expressed as the fold change of induced intracellular ROS.

2.5.5. Mutagenic frequency

The *in vitro* hypoxanthine guanine phosphoribosyl transferase (HPRT) mutation assay was performed in accordance with the OECD Guidelines for the Testing of Chemicals 476 (OECD 476, 2016). The assay measures the disruption of HPRT enzyme activity in mutant cells after PM exposure. It allows only the mutant cells to proliferate in the presence of the purine analogue 6-thioguanine (6-TG), which exerts a cytostatic effect by impending the metabolism of non-mutated cells. Chinese hamster lung fibroblast cells V79-4 (CCL-3, ATCC®, USA) were freshly thawed and subcultured at a density of 2×10^5 cells mL^{-1} in T-75 flasks (Corning®, USA) for 2–4 passages. For PM exposure, 4×10^4 cells were seeded in 12-well plates (Corning®, USA) and cultured for 24 h at 37 °C with 5 % CO_2. Following the incubation, the cells were exposed to a subcytotoxic concentration of PM (15 μg cm^{-2}) for 24 h at 37 °C with 5 % CO_2. At the same time, untreated cells were cultured in DMEM without FBS to serve as a negative control, while cells were treated with 0.1 mM of ethyl-methanesulfonate (EMS, Sigma-Aldrich, USA) to function as the positive control. Following a 24-hour exposure period, 2×10^5 cells were subcultured in T-75 flasks (Corning®, USA) in a CO_2 incubator maintained at 37 °C, allowing the phenotypic expression of the induced mutations for an additional 11-day period, with cells being split upon reaching confluence. On days 5 and 11, 100 cells per well were plated in 6-well plates for the concurrent CFE assay. To detect mutants, one million cells were subcultured in 6-well plates to facilitate the formation of colonies by the mutant cells. Three hours after seeding,

the cells were treated with 500 μg mL^{-1} of 6-TG. Following an eight- to nine-day incubation period in 6-TG-containing media, the mutant colonies were stained with Giemsa. The mutation frequency (MF) was calculated using equation 3 (Åkerlund et al., 2018).

$$MF = \left(\frac{\text{Average of number of mutant colonies in treatment}}{\text{CFE} \times \text{total cells seeded}}\right) \times 10^6 \quad (3)$$

2.5.6. CYP enzyme activation

To evaluate the activation of xenobiotic metabolizing pathways induced by PAHs after PM exposure, the activity of cytochrome P450 (CYP450) enzymes was investigated. In this study, Alkoxyresorufin-based assays were utilized, which are widely used for their relative simplicity, low cost, and direct measurement of catalytic activity (Burke et al., 1985). Specifically, 7-Ethoxyresorufin-O-deethylase (EROD) and 7-Benzyloxyresorufin-O-debenzylase (BROD) assays were employed to detect CYP1A and CYP1B (Genies et al., 2013; Heinrich et al., 2014) and CYP3A activity (Hagemeyer et al., 2010), respectively. The assay was performed in accordance with the protocol outlined by Hagemeyer et al. (2010) with minor adjustments.

In this study, Alkoxyresorufin substrates (EROD and BROD) were added after exposure, thereby catalyzing the O-dealkylation of the substrate. This reaction results in the cleavage of the alkyl group and the production of fluorescent resorufin. Following a 24-hour exposure to PM, the cells were washed with prewarmed PBS and trypsinized for harvesting. For the positive control, cells were exposed to 5 μM of Benzo [a]pyrene in DMEM/F12 without FBS for 1 h, followed by the same harvesting procedure. The collected cells were centrifuged at 0.2 g for five minutes at room temperature, and the supernatant was removed. The resulting dry pellets were stored at −80 °C overnight for lysis until enzyme activity assays were performed. To prepare the enzyme reaction mixtures, cells were thawed, and working solutions were made from stock solutions of 10 mM of EROD (16122, Cayman, USA) and BROD (SC-208301, Santa Cruz, Germany) in dimethyl sulfoxide (DMSO). These stock solutions were subsequently diluted to 10 μM in HBSS containing 0.1 % v/v TritonX-100. Following a thawing process, 500 μL of each working solution was added to the cells. The solutions were then vortexed for ten seconds and incubated at 37 °C in a CO_2 incubator for five minutes. The initiation of the reaction was facilitated by the addition of 250 μL of 1 mM nicotinamide adenine dinucleotide phosphate (NADPH) in Milli-Q water, followed by incubation at 37 °C for eight minutes. Subsequently, 150 μL of the cell suspension was transferred to a black 96-well plate (SC-204450, Santa Cruz, Germany). CYP450 activity induced by PM exposure was quantified by measuring Resorufin-associated fluorescence, using a multimode microplate reader (Varioskan™ Lux, Thermo Fisher Scientific, USA) with excitation and emission wavelengths set at 544 and 595 nm, respectively. EROD and BROD activities were normalized to metabolic cell equivalents (MCE) derived from the trypan blue assay data of the corresponding treatment wells. The results were expressed as pmol Resorufin × MCE^{-1} × min^{-1} as described by Heinrich et al. (2014).

2.5.7. Interleukin-8 (IL-8) release

After 4 and 24 h of PM exposure, the culture media were collected, and the supernatants without cell debris and particles in the medium were separated via centrifugation at 110 g for 10 min (Universal 320R, Hettich, Germany). The separated extracts were then stored at −80 °C until analysis. The secretion of the pro-inflammatory cytokine IL-8 in the supernatants was determined in a 96-well plate using an enzyme-linked immunosorbent assay (ELISA) according to the manufacturer's instructions (DY208, R&D Systems Inc., USA). The assay utilized 3,3́,5,5́-tetramethylbenzidine as the substrate, and the absorbances of each sample were measured at 450 and 540 nm using a microplate reader (Varioskan™ Lux, Thermo Fisher Scientific, USA). The concentration of IL-8 was subsequently calculated based on standard curves and expressed as pg mL^{-1}.

2.5.8. Statistical methods

All biological experiments were repeated three times, and the data were analyzed using GraphPad Prism version 9.3.1 (GraphPad Software, USA) with one-way analysis of variance and Dunnett's test for multiple comparisons with p-values < 0.05, <0.01, <0.001, and < 0.0001.

3. Results

3.1. Characterization of the combustion particles

3.1.1. Physical characterization of PM from the research ship engine

The particle size distribution for various fuels was determined for particle diameters ranging from 14 to 740 nm (Fig. S2). The results revealed that particles from all HFOs exhibited remarkably skewed size distributions, with the median diameters smaller than 50 nm (Table 2). In contrast, the particle size distribution for MGO was not skewed as much as HFOs' size distribution, with a median diameter of 67 nm. Notably, the particle size distributions of LS-HFO and HS-HFO_{SYN} showed a slightly bimodal distribution (Fig. S2), suggesting the occurrence of interparticle phenomena within the exhaust line, such as particle-to-particle coagulation (Hinds, 2011). The mass concentration of particles for each fuel type is shown in Table 2. Combustion of HS-HFO_{SYN} produced the highest particle mass concentration, followed by HS-HFO, LS-HFO, ULS-HFO_{AR}, and MGO. The particle mass concentrations of MGO and ULS-HFO_{AR} were notably lower compared to the other fuel types. The equivalent black carbon (eBC) concentrations for each fuel are presented in Table 2. The highest eBC mass concentration was observed for HS-HFO_{SYN} emissions, followed by LS-HFO, HS-HFO, MGO, and ULS-HFO_{AR}.

3.1.2. Physical characterization of PM in suspension

The physical characteristics of the suspended PM in the cell exposure medium were analyzed using dynamic light scattering (DLS). This method was employed to determine the hydrodynamic diameter, state of agglomeration, and stability of the particles. Overall, the hydrodynamic diameters of PM were larger than their corresponding mobility diameters (Fig. S2). As shown in Table 3, the hydrodynamic diameter of HFO PM and ranged between 260 and 400 nm, while those of PM from MGO were around 185 nm.

The polydispersity index (PDI), a quantitative measure of particle size distribution within the medium, revealed notable differences between the particles. The PDI of the HFO PM samples ranged from 0.21 to 0.34, indicating a relatively broad size distribution in the exposure medium. In contrast, MGO PM samples exhibited a narrower size distribution, with a PDI value below 0.2. To further investigate colloidal stability, the zeta potential of the PM was measured. Zeta potential, which reflects the surface charge of particles, provides insight into the repulsive forces between particles due to their surface charge. In the cell medium, the zeta-potential of MGO PM was measured at −18.6 mV, whereas HFO PM exhibited zeta potentials ranging from −11.9 mV to

Table 2
Total particle and eBC mass concentrations as well as median and mean diameter of the size distribution from the exhaust emissions of each fuel type during the engine cycle are given in mg m^{-3} and nm, respectively, with standard deviations from three independent experiments (n = 3).

	MGO	ULS-HFO_{AR}	LS-HFO	HS-HFO_{SYN}	HS-HFO
Mass concentration	10 ± 2	12 ± 1	30 ± 9	79 ± 4	48 ± 6
eBC concentration	10 ± 3	7 ± 1	23 ± 2	43 ± 2	16 ± 2
Median diameter	67 ± 3	27 ± 1	31 ± 1	34 ± 1	41 ± 1
Mean diameter	88 ± 2	40 ± 1	53 ± 1	57 ± 1	52 ± 1

Table 3
Results of DLS measurement in the exposure medium. All parameters are presented with standard deviations of three measurements.

	MGO	ULS-HFO_{AR}	LS-HFO	HS-HFO_{SYN}	HS-HFO
	Exposure medium (DMEM/F12)				
Diameter [nm]	185 ± 2	310 ± 8	286 ± 4	398 ± 9	262 ± 8
PDI [-]	0.18 ± 0.01	0.3 ± 0.03	0.21 ± 0.01	0.34 ± 0.03	0.28 ± 0.02
Zeta-potential [mV]	−18.6 ± 2.1	−14.5 ± 1.0	−13.6 ± 1.7	−14.2 ± 1.0	−11.9 ± 1.3

−14.5 mV.

3.1.3. Chemical composition and mutagenic equivalent of the collected PM

The mass concentrations of 12 targeted PAHs, the mutagenic equivalent factor (MEF) of each PAH, and the sum of the PAH and Benzo[a]pyrene-related mutagenic equivalency values (BaPMEQ) are shown in Table 4 and Fig. S3 as a bar graph. The dominant PAHs in the combustion PM of all fuel types were Pyrene, Chrysene, and Fluoranthene. The PM from ULS-HFO_{AR} exhibited an abundant emission profile of Fluoranthene, Pyrene, and Benz[a]anthracene, while HS-HFO_{SYN} PM had the highest overall PAH concentrations. HS-HFO PM demonstrated moderate concentrations of PAH concentrations across most measured compounds, while MGO PM displayed at least one order of magnitude lower concentrations. The sum of BaPMEQ (∑BaPMEQ) revealed notable variations in the mutagenic potential of PM emissions across different marine fuel types (Table 4). The ∑BaPMEQ values of PM from all HFO fuel types were approximately 100 times higher than those of MGO PM. Among the various HFO PMs, HS-HFO_{SYN} PM exhibited the highest total BaPMEQ, measuring 93 ng mg^{-1}. A substantial proportion of this total, exceeding 70 %, consisted of Benz[a]anthracene, Benzo[a]pyrene, Benzo[b]fluoranthene, and Benzo[ghi]perylene. A similar trend was observed in other HFO PMs, which also exhibited high concentrations of Benzo[a]pyrene and Benzo[b]fluoranthene. Although MGO PM exhibited a composition dominated by Benzo[a]pyrene and Benzo[b]fluoranthene, accounting for over 60 % of the ∑BaPMEQ, the low PAH concentrations led to a substantially diminished ∑BaPMEQ.

Table 4
PM-bound PAHs, mutagenic equivalency factor (MEF) of 12 targeted PAHs (Durant et al., 1996) with standard deviations of three independent experiments (n = 3) and the sum of the mutagenic equivalent values (BaPMEQ) of the combustion PM from each fuel type.

PAH [ng mg^{-1}]	MEF	MGO	ULS-HFO_{AR}	LS-HFO	HS-HFO_{SYN}	HS-HFO
Fluoranthene	0	2.4 ± 0.4	240 ± 25	77 ± 9.5	170 ± 18	110 ± 15
Pyrene	0	2.6 ± 0.6	330 ± 30	88 ± 10	330 ± 31	170 ± 20
Benz[a]anthracene	0.082	0.8 ± 0.1	85 ± 9.1	75 ± 11	100 ± 6.7	59 ± 6.6
Chrysene	0.017	2.8 ± 0.5	250 ± 24	200 ± 41	270 ± 21	180 ± 23
Benzo[b]fluoranthene	0.25	0.5 ± 0.1	30 ± 3.7	66 ± 12	83 ± 3.6	50 ± 6.2
Benzo[k]fluoranthene	0.11	0.03 ± 0.02	4.0 ± 0.5	14 ± 2.8	18 ± 1.1	11 ± 1.4
Benzo[e]pyrene	0.0017	0.3 ± 0.04	22 ± 3.3	58 ± 11	140 ± 12	63 ± 8.1
Benzo[a]pyrene	1	0.1 ± 0.05	6.3 ± 1.6	21 ± 6.0	40 ± 1.5	31 ± 6.0
Perylene	0	< LOQ	1.3 ± 1.0	8.0 ± 3.3	6.7 ± 0.9	4.4 ± 0.4
Indeno[1,2,3-cd]pyrene	0.31	< LOQ	1.8 ± 0.6	9.4 ± 3.0	18 ± 0.9	9.8 ± 1.7
Benzo[ghi]perylene	0.19	< LOQ	2.6 ± 0.8	17 ± 4.0	51 ± 1.1	23 ± 3.9
Dibenz[a,h]anthracene	0.29	< LOQ	1.0 ± 0.3	4.0 ± 0.9	7.7 ± 0.2	3.4 ± 0.6
∑PAH [ng mg^{-1}]		9.6 ± 0.8	974 ± 47	637 ± 48	1234 ± 44	715 ± 37
∑BaPMEQ [ng mg^{-1}]		0.34 ± 0.1	27 ± 2.1	56 ± 6.9	93 ± 1.9	61 ± 6.3

< LOQ- Limit of quantification

In addition to analyzing the PAH content, the elemental composition of PM was determined using ICP-OES. As shown in Table 5, elevated concentrations of Vanadium and Sulfur per unit of PM mass were observed with higher FSC, while Zinc and Calcium concentrations in the exhaust exhibited an inverse trend. Notably, ULS-HFO_{AR} PM exhibited substantially higher concentrations of Zinc and Calcium relative to PM mass. Iron and Nickel concentrations did not show any significant variation among PM from different fuel types, except for ULS-HFO_{AR} PM, which exhibited the lowest Nickel concentration. It is important to note that elemental analysis of MGO PM was not feasible due to the limited amount of PM collected. However, previous studies have demonstrated that the emission factors of transition metals (Fe, Ni, and V) from MGO combustion are significantly lower compared to those from HFO combustion (Table S3) (Sippula et al., 2014; Oeder et al., 2015; Lunde Hermansson et al., 2021; Sueur et al., 2023). The results of the elemental analysis of all compounds normalized to PM mass are shown in Table S4.

3.2. $PM_{2.5}$-induced toxicological responses

3.2.1. Cell viability and clonogenicity

As shown in Fig. 2a and 2b, exposure to PM for 4 and 24 h led to only a minor decrease in cell viability across most fuel types and concentrations compared to the control group. No significant changes in cell viability were observed for the lowest and intermediate concentrations of PM, suggesting their limited cytotoxic potential at these levels. However, exposure to the highest concentration of LS-HFO PM resulted in a significant reduction in cell viability at both time points, with a viability decreasing to 85 %. The findings from the trypan blue assay support further investigation into the effects of subtoxic particle concentrations. These results could help distinguish whether the observed responses stem from toxic conditions associated with elevated particle concentrations or from the activation of specific cellular pathways under sublethal stress conditions.

The CFE assay is widely recognized as being more sensitive than other cell viability assays, such as the trypan blue assay, for detecting subtle biological responses (Ponti et al. 2014). For this reason, it was selected to assess cell clonogenicity in this study. The enhanced sensitivity of the CFE assay was evident in our experiment, as shown in Fig. 2c and 2d. After 4 h of exposure (Fig. 2c), HS-HFO_{SYN} PM significantly reduced CFE at both intermediate and high concentrations. Interestingly, MGO PM induced approximately a 10 % increase in CFE by at the lowest particle concentration, a response not observed with PM from other fuel types at this level. Contrary to expectations based on the acute cell membrane disruption seen in the trypan blue assay, LS-HFO PM exhibited only a slight, concentration-dependent decrease in CFE, which was not statistically significant. Prolonged exposure led to more pronounced cytotoxic effects, particularly for fuels with higher FSC

Table 5
Elemental mass concentrations from the exhaust emission of each fuel type during the engine cycle expressed as μg mg^{-1} with the uncertainty of the instrumental analysis.

[μg mg^{-1}]	ULS-HFO_{AR}	LS-HFO	HS-HFO_{SYN}	HS-HFO
Calcium (Ca)	45 ± 0.4	23 ± 0.2	10 ± 0.1	6.6 ± 0.07
Iron (Fe)	5.7 ± 0.03	4.3 ± 0.03	4.2 ± 0.03	5.1 ± 0.03
Nickel (Ni)	1.2 ± 0.01	6.2 ± 0.08	8.3 ± 0.1	5.9 ± 0.07
Sulfur (S)	29 ± 0.2	39 ± 0.3	28 ± 0.2	41 ± 0.3
Vanadium (V)	5.4 ± 0.2	14 ± 0.4	13 ± 0.4	24 ± 0.7
Zinc (Zn)	1.8 ± 0.02	0.7 ± 0.01	0.50 ± 0.01	0.20 ± 0.01

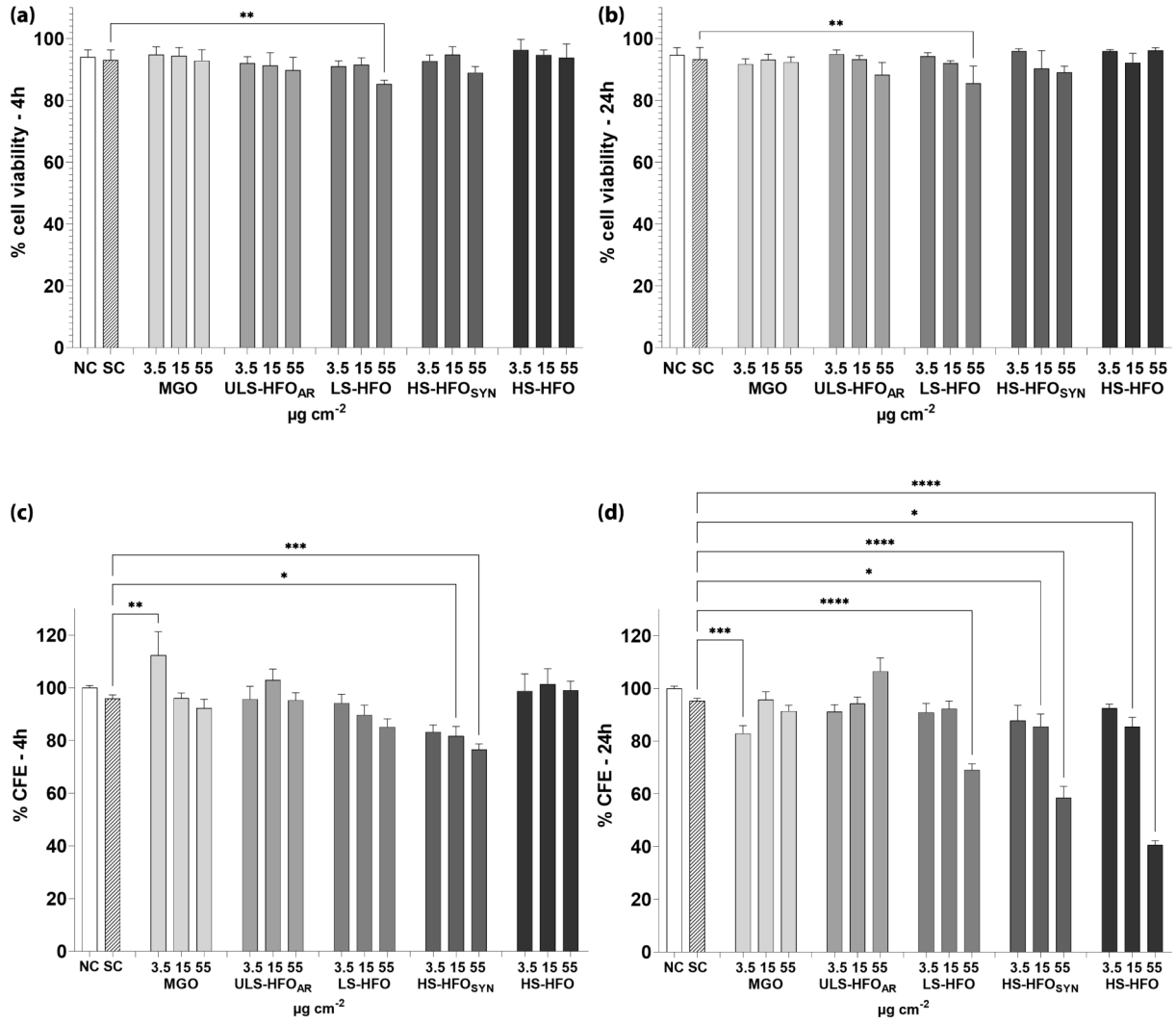

Fig. 2. A549 cell viability and clonogenicity after exposure to different concentrations (3.5, 15, and 55 µg cm^{-2}) of PM from marine fuel emissions. NC, negative control; SC, solvent control. Cell viability following (a) 4 and (b) 24 h exposure. % CFE following (c) 4 and (d) 24 h exposure Results are presented as mean ± SEM from three independent experiments (n = 3; *$p < 0.05$; **$p < 0.01$; ***$p < 0.001$; ****$p < 0.0001$ vs. SC.

(Fig. 2d). At the highest concentration, LS-HFO, HS-HFO$_{SYN}$, and HS-HFO PM reduced CFE to approximately 70 %, 60 %, and 40 %, respectively. Additionally, the intermediate concentrations of HS-HFO$_{SYN}$ and HS-HFO PM reduced clonogenicity to around 85 %. Notably, while MGO PM initially caused a 10 % increase in CFE after 4 h, it induced a significant reduction in CFE to 80 % after 24 h at the same concentration. No reduction in CFE was observed with MGO at other concentrations following 24 h exposure.

3.2.2. *Genomic instability, intracellular ROS, and gene mutation*

PM exposure has been shown to disrupt the oxidant-antioxidant balance, leading to DNA damage, gene mutations, and chromosomal aberrations (Fresta et al., 2018; Cao et al., 2022; Cho et al., 2022). Among these, DNA strand breaks are considered one of the most severe forms of DNA damage. As illustrated in Fig. 3a and 3b, a dose-dependent increase of DNA damage was observed after 4 and 24 h of exposure. Notably, the percentage of DNA breaks significantly increased with prolonged exposure, particularly for high sulfur-containing HFOs. Baseline levels of DNA breaks were evaluated in both negative and solvent controls, with approximately 3 % detected for both exposure durations, and no significant differences observed between the controls.

Following a 4-hour exposure, MGO and ULS-HFO$_{AR}$ PM showed a dose-dependent increase of genotoxic effects. However, significant DNA damage was only observed at the highest concentration of MGO PM. In contrast, high sulfur HFO PMs (HS-HFO$_{SYN}$ and HS-HFO) caused significant DNA damage at the highest concentration, with HS-HFO$_{SYN}$ inducing notable effects at the intermediate concentration (Fig. 3a). LS-HFO PM did not cause significant DNA damage after 4 h, though a slight increase in DNA damage was observed at higher concentrations. After 24 h of exposure, significant DNA damage was observed for all high sulfur-containing HFO PM and LS-HFO PM at the highest concentration (Fig. 3b). Interestingly, HS-HFO PM induced significant DNA damage at the intermediate concentration. This finding suggests a possible role of sulfur, or other chemical compounds, associated with high FSC in the observed reduction in cell viability and increase in DNA damage, which deserves further investigation to clarify their roles and underlying mechanisms. Notably, the substantial DNA damage induced by MGO PM after 4 h was reduced after 24 h, with decreases in DNA damage observed at the intermediate and highest concentrations of MGO PM. As shown in Fig. 3c, intracellular ROS levels induced by PM exposure were measured through kinetic fluorescence intensity over a 4-hour exposure period. An increase in intracellular ROS was observed with increasing concentrations of all PM types. Significant ROS increases were recorded for MGO, ULS-HFO$_{AR}$, and HS-HFO PM at the highest concentration, with 4.3-, 2.5-, and 4-fold increases, respectively. In contrast, exposure to LS-HFO (1.6-fold) and HS-HFO$_{SYN}$ (1.4-fold) PM resulted in a slight

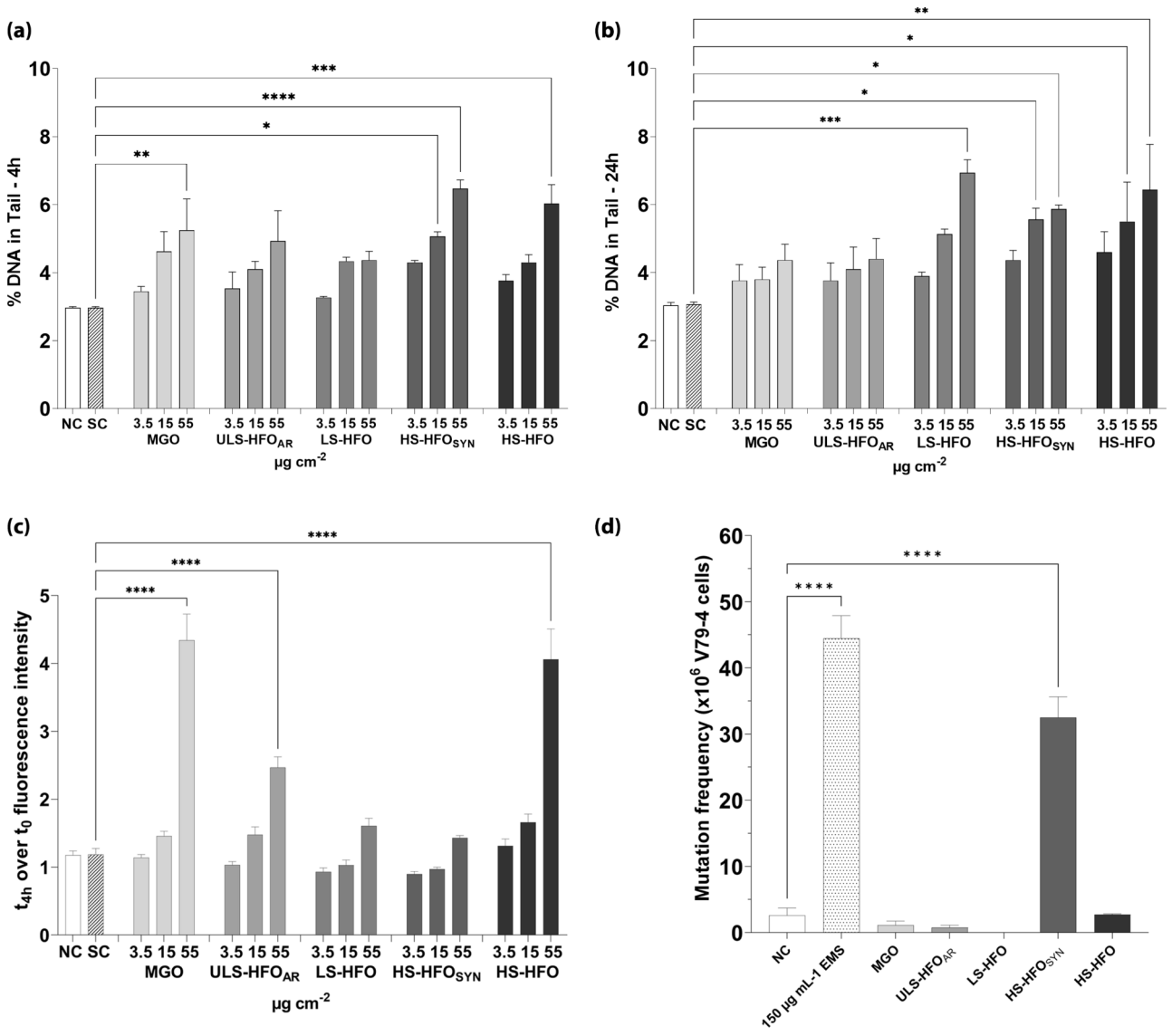

Fig. 3. DNA damage, intracellular ROS, and V79-4 cell mutagenicity after exposure to different concentrations (3.5, 15, and 55 µg cm^{-2}) of PM from marine fuel emissions. NC, negative control; SC, solvent control. DNA strand breaks measured using comet assay and represented as percentage of DNA damage in tail of A549 cells after 4 (a) and 24 h (b) exposure. (c) Intracellular ROS formation calculated as fold change of the fluorescence intensity kinetics in A549 cells over 4 h exposure. (d) HPRT gene mutation frequency in V79-4 cells after 24 h exposure to 15 µg cm^{-2} of marine fuel PM. Results are presented as mean ± SEM from three independent experiments (n = 3). *$p < 0.05$; **$p < 0.01$; ***$p < 0.001$; ****$p < 0.0001$ vs. SC (a, b, and c) or NC (d) for the mutation frequency.

but non-significant ROS increases. Interestingly, the ROS trends for HFO PMs aligned with the aromatic content of the fuels, suggesting that oxidative stress may be influenced by specific PAH components. However, the contrasting trend for MGO PM, which contains a very low concentration of PAH compounds, indicates that other factors, such as particle size, may play a critical role in ROS induction. Given the observed cytotoxic, genotoxic, and oxidative stress induced by PM exposure, the mutagenic potential of PM was evaluated. Mutagenicity, which can arise directly or indirectly from inadequate DNA repair or severe DNA breaks (Cho et al., 2022), was assessed using the HPRT assay with V79-4 cells. As shown in Fig. 3d, only HS-HFO$_{SYN}$ PM exhibited a significant increase in mutagenic frequency despite comparable levels of DNA damage induced by LS-HFO and HS-HFO PMs. This suggests that HS-HFO$_{SYN}$ PM may uniquely influence the pathways leading to mutagenesis.

3.2.3. CYP enzymes activity and IL-8 release

The presence of PM from aromatic-rich fuel types (ULS-HFO$_{AR}$, HS-HFO$_{SYN}$, and HS-HFO) significantly activated EROD activity at the highest concentration (Fig. 4a). In contrast, while MGO and LS-HFO PM showed a slight dose-dependent increase in fluorescence intensity, these changes did not reach statistical significance. In the BROD assay, only HS-HFO PM, one of the aromatic-rich fuel types, significantly induced BROD activity at the highest concentration (Fig. 4b). Although the other aromatic-rich fuels displayed activation of BROD, these increases were not statistically significant. Conversely, MGO and LS-HFO PM demonstrated no induction of BROD activity. Overall, the lack of significant EROD and BROD activation by MGO and LS-HFO PM is notable, especially given the relatively lower PAH concentrations associated with these fuels compared to other HFOs. To further investigate the relationship between CYP450 induction and PM exposure, the release of the pro-inflammatory factor Interleukin-8 (IL-8) was examined. As shown in Fig. 4c and 4d, IL-8 release was measured after 4 and 24 h of exposure to PM at a sub-cytotoxic particle concentration (15 µg cm^{-2}). This concentration was selected based on the trypan blue and CFE results, ensuring that cell viability remained above 80 % while minimizing the

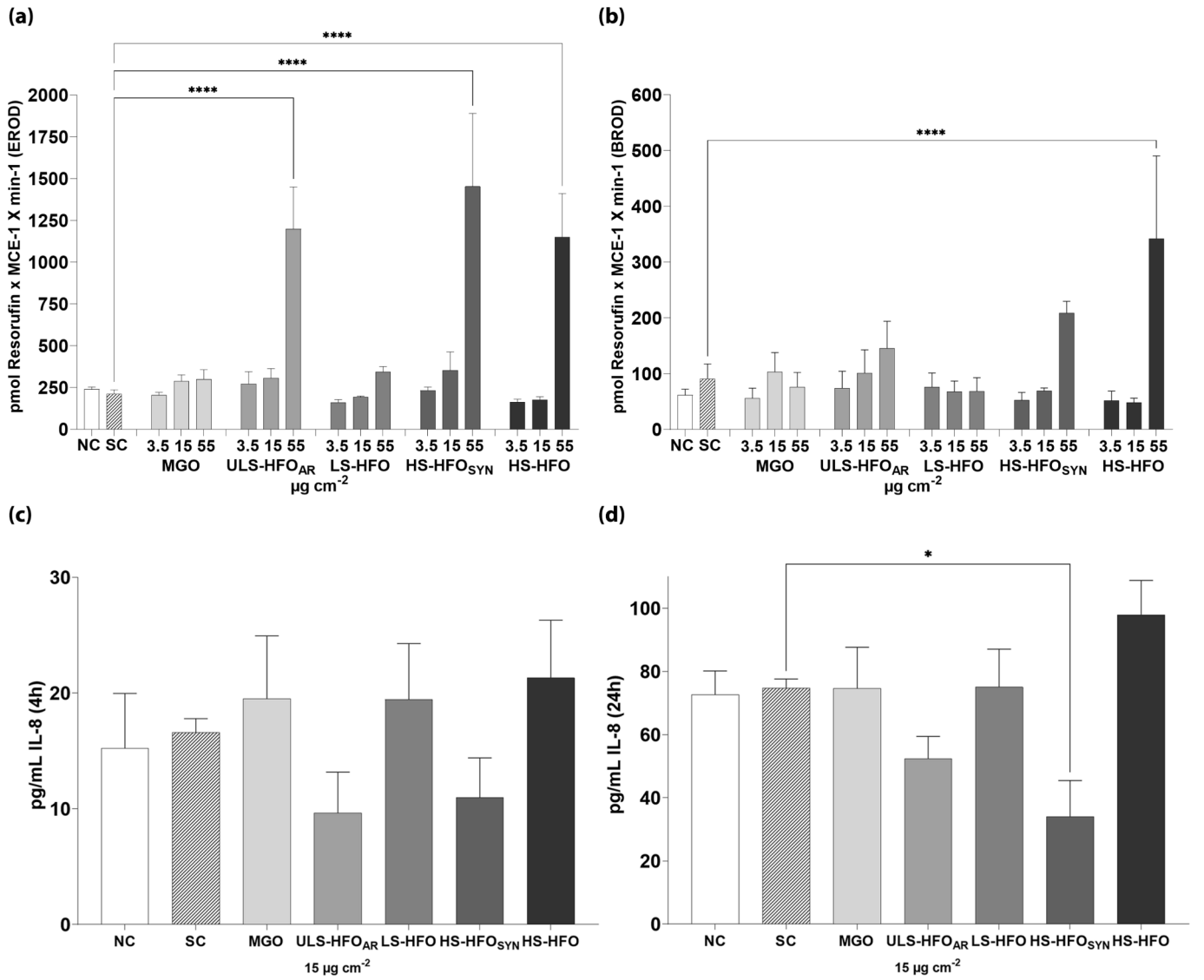

Fig. 4. Induction of the Resorufin intensity from 7-Ethoxyresorufin-O-deethylase (EROD) (a) and 7-Benzyloxyresorufin-O-debenzylase (BROD) (b) in A549 cells normalized by metabolic cell equivalent (MCE) and exposure time to different concentrations (3.5, 15, and 55 µg cm^{-2}) of PM from marine fuel emissions. The release of the pro-inflammatory cytokine IL-8 in A549 cells exposed to 15 µg cm^{-2} of marine fuel PM for 4 h (c) and 24 h (d). Data are shown as the mean + SE (n = 3). Statistically significant with respect to the solvent control according to one-way ANOVA with Dunnett's test. *$p < 0.05$; **$p < 0.01$; ***$p < 0.001$; ****$p < 0.0001$ vs. the solvent control.

likelihood of artificially low IL-8 release due to reduced cell numbers. After 4 h of exposure, no statistically significant increase in IL-8 release was observed for PM from any fuel type (Fig. 4c). Similarly, after 24 h of exposure, no statistically significant increase in IL-8 release was detected. However, HS-HFO_{SYN} PM showed a significant suppression of IL-8 release (Fig. 4d). Additionally, ULS-HFO_{AR} PM, another aromatic-rich fuel type, showed a slight but non-significant suppression of IL-8 release. These findings suggest that while PM exposure induces CYP450 activity, it does not consistently elicit IL-8-mediated pro-inflammatory responses, particularly under sub-cytotoxic conditions. To facilitate comparison, the observed biological responses, including cytotoxicity, clonogenicity, genotoxicity, mutagenicity, oxidative stress, xenobiotic metabolism and pro-inflammatory responses, resulting from PM exposure across five marine fuels are summarized in Table 6.

Table 6
Summary of biological responses to PM exposure from five marine fuels at two exposure periods (4 and 24 h). Arrows represent statistically significant increases or decreases.

Effect	MGO		ULS-HFO_{AR}		LS-HFO		HS-HFO_{SYN}		HS-HFO	
Exposure Time	4	24	4	24	4	24	4	24	4	24
Cell viability	–	–	–	–	↓	↓	–	–	–	–
Clonogenicity	↑	↓	–	–	–	↓	↓	↓	–	↓
Genomic Instability	↑	–	–	–	–	↑	↑	↑	↑	↑
Intracellular ROS	↑		↑		–		–		↑	
Gene Mutation		–		–		–		↑		–
EROD-Activity		–		↑		–		↑		↑
BROD-Activity		–		–		–		–		↑
IL-8 Release	–	–	–	–	–	–	–	↓	–	–

4. Discussion

Extensive research has demonstrated that marine fuels emit a diverse array of gaseous and particulate pollutants with varying physical and chemical properties. While numerous studies have emphasized the benefits of low-sulfur marine fuels, these investigations have primarily focused on the physical and chemical characteristics of emitted pollutants (Moldanová et al., 2013; Lehtoranta et al., 2019; Kuittinen et al.,

2021). Current regulations, however, are centered predominantly on FSC compliance. This allows for the formulation of diverse fuel blends with distinct properties, as long as they meet FSC limits. As a result, various fuel types are now available, yet there is a significant lack of research into their toxicological impacts. To address this gap, the present study conducted a comprehensive investigation of PM emissions from five different marine fuel types under controlled laboratory conditions using a research ship engine. In parallel, a wide range of biological responses was evaluated to establish links between the properties of emitted PM and their toxicological effects.

The particle size distributions directly measured in the exhaust gases revealed distinct patterns between fuel types. Specifically, all emissions from HFO combustion exhibited skewed size distributions, whereas the size distribution of MGO PM showed a normal distribution. Additionally, higher Sulfur content in HFO was associated with increased particle number and mass concentrations in the emissions. These findings align with those of a previous study (Jeong et al., 2023), which attributed the elevated particle emission from HFOs to incomplete combustion processes and the formation of Sulfuric acid particles, both driven by the inherent properties of HFO fuels (Zetterdahl et al., 2016; Lehtoranta et al., 2019). The high PM mass concentration observed for HFO fuels were accompanied by elevated eBC concentrations, which reflects a greater contribution of light-absorbing carbonaceous material. While eBC alone does not fully characterize combustion completeness, the observed trend may indicate less efficient combustion for these fuels. These findings are consistent with earlier experiments, particularly the low eBC levels observed for HS-HFO (Jeong et al., 2023). This observation is further supported by another study, which reported a lower elemental carbon (EC) emission factor for HS-HFO PM compared to HS-HFO_{SYN} and LS-HFO PM (Bauer et al., 2024). The study attributed the higher EC emission factor of HS-HFO_{SYN} to its discontinuous boiling behavior, a characteristic evident in the boiling distribution profiles of the tested fuels (Fig. S1). Furthermore, the elevated Sulfur and metal content present in HS-HFO has been shown to inhibit soot formation while promoting EC oxidation (Wang et al., 2010). This finding underscores that the chemical composition of marine fuels, beyond their sulfur content, plays a significant role in shaping their emission profiles.

In this study, cells were exposed to particles suspended in the cell culture medium, which significantly altered the physical properties of the particles, such as size distribution. This effect can be attributed to protein corona formation, a phenomenon that dynamically influences particles agglomeration in biological media by altering their size and surface properties (Walczyk et al., 2010). To account for these changes, the physical properties of all PM types were analyzed using dynamic light scattering (DLS) prior to cell exposure. Notably, MGO PM exhibited the largest mode diameter (~60 nm) in the exhaust gas, which increased moderately to 185 nm in the cell culture medium. In contrast, HFO PMs, characterized by smaller mode diameters (< 50 nm) in exhaust gas, underwent a substantial increase in hydrodynamic diameter, ranging from 260 to 398 nm. This pronounced size increase reflects a greater tendency for particle agglomeration in the cell medium, consistent with previous observations (Halamoda-Kenzaoui et al., 2017; Kendall et al., 2015). Additionally, MGO PM exhibited the lowest polydispersity index (PDI), indicating a more monodisperse particle distribution compared to HFO PMs, which displayed higher PDI values and larger hydrodynamic diameters. These findings suggest a more heterogeneous aggregation behavior for HFO PMs. Zeta potential measurements further supported these observations: MGO PM demonstrated the highest zeta potential, signifying stronger interparticle electrostatic repulsion. This repulsion contributes to their smaller hydrodynamic diameter and reduced aggregation tendency (Kendall et al., 2015). In contrast, HFO PMs exhibited lower zeta potential values, which reduce the net surface charge, weaken electrostatic repulsion, and enhance aggregation, consistent with their broader size distribution and higher PDI. Based on the DLS results, the stable dispersion of MGO PM is expected to enhance intracellular internalization, aligning with observations reported by dos Santos et al. (2011). However, the potential internalization of larger, aggregated HFO PMs cannot be excluded. PAHs detached from these particles may interact with cellular receptors, such as the aryl hydrocarbon receptor (AhR), initiating redox responses, oxidative damage, and inflammation. This interaction could result in cytotoxic, genotoxic, and mutagenic effects, or non-malignant physio-pathological responses depending on the chemical properties of the PAHs (Låg et al., 2020). Among the PMs collected from different marine fuel types, HS-HFO_{SYN} PM exhibited the highest sum of PAH concentrations, followed by ULS-HFO_{AR} PM, highlighting the potential of HFOs to exhibit a wide range of aromatic properties irrespective of their Sulfur content. In contrast, MGO PM contained significantly lower concentrations of PAHs, approximately two orders of magnitude lower than those observed in HFO PMs, consistent with previous findings (Streibel et al., 2017). Interestingly, ULS-HFO_{AR} PM showed comparable, and in some cases higher, concentrations of medium-molecular-weight (MMW, 200 g mol^{-1} < MW < 250 g mol^{-1}) PAHs compared to HS-HFO_{SYN} PM. This observation suggests that ULS-HFO_{AR} PM may have initially contained higher levels of low-molecular-weight (LMW, MW < 200 g mol^{-1}) PAHs, which likely evaporated due to their higher vapor pressure, leading to their absence in the particle phase, as reported by Yang et al. (2021). This hypothesis is further supported by the relatively lower contribution of Fluoranthene and Pyrene compared to the results of previous studies (Sippula et al., 2014; Czech et al., 2017). These discrepancies may be attributed to the presence of untargeted alkylated derivatives of PAHs and the extended sampling duration, which could have led to the loss of more volatile species due to blow-off effects. Such factors likely contributed to the higher Calculated Carbon Aromaticity Index (CCAI) and Aromaticity Index (AI) of the fuels, as shown in Table 1, while LMW-PAHs were largely absent from the particle phase. Other HFO PMs, such as LS-HFO and HS-HFO, exhibited lower LMW-PAH concentrations compared to ULS-HFO_{AR} PM, while their HMW-PAH concentrations fell between those of ULS-HFO_{AR} PM and HS-HFO_{SYN} PM, consistent with their respective fuel properties. In addition to organic compounds, inorganic compounds also contribute significantly in shaping the properties of PMs and their effects on cells (Akhtar et al., 2014). The most pronounced differences in inorganic composition were observed between HFO PMs and MGO PM as shown by Streibel et al. (2017). This discrepancy can be attributed to the refining processes of crude oil, where the distillation of organic fractions enriches metals and low-boiling organic compounds in the residual oil. Emissions of transition metals, including Nickel (Ni), Iron (Fe), and Vanadium (V), are predominantly fuel-derived and associated with the high-boiling fractions of crude oil (Quimby et al., 1991). However, their concentrations can vary widely depending on the crude oil source. Interestingly, our findings revealed that Fe concentrations remained relatively consistent across the different fuel types, while Ni and V concentrations were lowest in ULS-HFO_{AR} PM. In addition, it is noteworthy that the sulfur concentrations of PM do not correlated with the sulfur content of the fuels. During the combustion process, sulfur in the fuel is oxidized, forming SO_2 and, to a lesser extent, SO_3. These oxides contribute to PM emissions in the form of sulfates. Sarvi et al. (2011) identified additional factors that influence this process, including oxygen availability and the catalytic activity of metals such as V and Ni, which enhance the oxidation of SO_2 to SO_3, thereby increasing sulfate formation.

In addition to fuel-derived fractions, metal compounds can originate from lubricant oil, such as Calcium (Ca) and Zinc (Zn), which are commonly detected in PM (Okada et al., 2003). Increased fuel consumption and higher combustion temperatures in engines are associated with greater lubricant oil usage, contributing to these metal emissions (Sarvi et al., 2011). Interestingly, in this study Zn and Ca concentrations were observed to decrease with increasing FSC. This finding suggests that high sulfur-containing HFO, due to its inherently high viscosity, required additional lubricant oil to maintain optimal combustion conditions. The increased lubricant use may have diluted the HFO, resulting in unexpected trends in the transition metal composition of HFO PMs.

Although variations in the transition metal compounds were less pronounced than those observed in the organic fractions, further research is necessary to clarify the interplay between fuel consumption, combustion conditions, engine operation, and catalytically active metals in shaping PM characteristics. Additionally, investigating the mechanisms underlying sulfur oxidation and sulfate formation, particularly in the presence of transition metals, is essential for a more comprehensive understanding of these processes.

To evaluate the toxicological effects of PMs chemical composition, particles were dispersed in the medium at controlled mass concentrations. The cell viability analysis revealed only minor effects, which were exclusively associated with LS-HFO PM at the highest concentration for both exposure times (4- and 24-hours). However, the clonogenicity assessment showed a dose- and time-dependent decrease, particularly after prolonged exposures to HFO PMs. This time-dependent reduction in clonogenicity aligns with previous studies that demonstrated increased PM uptake by cells and greater release of organic and inorganic compounds from PM during extended exposure periods (Corbin et al., 2018; Di Bucchianico et al., 2017; Zerboni et al., 2019). The differential effects observed among HFO PMs can be attributed to variations in PM-bound PAH concentrations, particularly high molecular weight (HMW)-PAHs such as Benzo[a]pyrene, Benzo[b]fluoranthene, and Benzo[ghi]perylene (Table 4). Similar reductions in cell viability linked to PAH concentrations have been reported in studies involving PM from the combustion of petrol and diesel fuels (Wu et al., 2017). Interestingly, exposure to MGO PM at the lowest concentration resulted in a slight increase in clonogenicity after 4 h of exposure, which subsequently decreased to approximately 80 % after 24 h. This finding aligns with observations by Guéguen et al. (2018), who reported adaptive cellular responses to low-dose chemical exposures. These responses transiently enhance cellular survival mechanisms but are eventually overwhelmed during prolonged exposure, leading to reduced viability. Similarly, Fresta et al. (2018) proposed that such responses may result from fundamental metabolic changes, including imbalances in adenine nucleotide homeostasis and mitochondrial dysfunction, which are induced by non-cytotoxic particle concentrations. Regarding the reduction in cell viability, the PM samples can be broadly categorized into two groups: low sulfur-containing fuel PM (MGO and ULS-HFO_{AR}), which did not significantly affect cell viability or proliferation, and high sulfur-containing fuel PM (LS-HFO, HS-HFO_{SYN}, HS-HFO), which induced pronounced cytotoxicity. These findings are consistent with previous studies indicating higher cytotoxicity of HFO emissions compared to diesel-like fuels, both at the air–liquid interface (Oeder et al., 2015) and under submerged cell culture conditions (Wu et al., 2018). In addition to assessing cell viability, the presence of PAHs in these PMs has been shown to induce genotoxic effects through metabolic activation. This process generates reactive metabolites that can covalently bind to DNA leading to oxidative lesions mediated by oxidative stress. Oxidative stress inhibits polymerase activity, impairs DNA repair mechanisms, and ultimately causes genotoxicity. Over time, these processes can lead to an accumulation of mutations, potentially contributing to carcinogenesis (Hsu et al., 2005; Munoz and Albores, 2011). Previous investigations have examined the role of PAHs in reducing cell viability and increasing DNA damage. Bonetta et al. (2009) reported that organic extracts from $PM_{2.5}$ significantly increased DNA damage in A549 cells in a dose-dependent manner, correlating the observed genotoxic effects with the high content of carcinogenic PAHs. Another study exposed A549 cells to organic extracts of traffic-related PM and found that high concentrations of PAHs significantly reduced cell viability and increased DNA damage (Shang et al., 2013). These findings suggest that the cytotoxic and genotoxic effects induced by high PAH-containing PM are related to intracellular ROS generation. Notably, the DNA damage induced by the highest concentration of MGO PM after 4 h of exposure was resolved after 24 h, suggesting an adaptive cellular response similar to that observed for cell viability (Fig. 2c, 2d). This resolution can likely be attributed to the activation of DNA repair mechanisms during prolonged exposure. Since PAH-induced cytotoxicity and genotoxicity are often linked to oxidative stress, particularly through reactive metabolites formed during the detoxification/metabolizing processes (Shimada and Fujii-Kuriyama, 2004), intracellular ROS play a pivotal role in cell damage and are an important precursor to subsequent underlying mechanisms. In this study, increases in ROS levels were observed with increasing concentrations of all PMs. However, it is noteworthy that only certain fuel types, namely MGO, ULS-HFO_{AR}, and HS-HFO PM, induced a significant ROS response at the higher concentration.

On the one hand, the observed trend for intracellular ROS in HFO PMs was largely consistent with their aromatic-rich fuel types, supporting the hypothesis that oxidative stress may be primarily driven by PAHs bound to and released from PM during exposure. On the other hand, an exception was observed with the HS-HFO_{SYN} PM, which, despite containing the highest concentration of aromatic compounds, did not induce intracellular ROS to a significant extent. While the potential role of transition metals, such as Vanadium, and the complex chemical composition of PM, including humic-like substances, in the generation of intracellular ROS cannot be completely excluded, as supported by numerous studies (Win et al., 2018; Schneider et al., 2023; Sueur et al., 2023), identifying their specific contribution is challenging due to the relatively minor differences in their concentrations between fuel types (Table 5). Consequently, this unexpected finding may be attributed to potential perturbations or inefficiencies in the metabolizing pathways specific to HS-HFO_{SYN} PM. Interestingly, MGO PM induced significant intracellular ROS at the highest concentration, despite its lower PAH and metal content compared to HFO PMs. This phenomenon may be linked to their smaller particle size in suspension relative to other PMs (Table 3). It is well known that smaller particles enhance intracellular internalization, which subsequently influences ROS generation. This finding is consistent with previous observation that cellular uptake of particles is highly size-dependent for a variety of cell lines including A549 (dos Santos et al., 2011). The strong intracellular ROS induction by MGO PM within a 4-hour exposure period is also consistent with the observed changes in DNA damage over the same period. However, a mitigated DNA damage response was observed after 24 h of exposure, which may be attributed to the presence of intact and functional DNA repair mechanisms. While these mechanisms initially counteract the damage, the persistent ROS induction by PM and PM-bound PAHs, leading to oxidative stress and DNA adduct formation, suggests that prolonged exposure to significant concentrations or specific chemical compounds may overwhelm cellular repair systems, increasing mutagenic potential (Cho et al., 2022). In our study, the mutagenic potential of each PM was assessed using the HPRT assay, which revealed that HS-HFO_{SYN} PM induced significant mutagenicity. This was consistent with its remarkably high mutagenic risk assessed by BaP equivalents. These findings support our hypothesis that certain chemical compounds in PM may disturb specific xenobiotic metabolizing pathways or cell cycle progression, leading to the preferential formation of DNA adduct-forming intermediates rather than ROS, which ultimately increases mutation rates. Despite relatively low ROS production by HS-HFO_{SYN} PM, a significant upregulation of AhR-related metabolizing enzymes was observed, as measured by EROD activity. This observation aligns with previous studies showing that exposure to PAH-rich PM significantly increases the expression of AhR-regulated genes (Billet et al., 2007; Gualtieri et al., 2012). For instance, Shimada and Fujii-Kuriyama (2004) reported significant activation of cyp1a1 and cyp1a2 enzymes in mouse liver cells exposed to high concentrations of chrysene, a compound abundant in ULS-HFO_{AR} and HS-HFO_{SYN} PM in this study. Similarly, Kim et al. (2003) demonstrated that Benzo[a]pyrene and Benz[a]anthracene significantly contribute to increased EROD activity in *in vivo* studies. Arrieta et al. (2003) further showed that organic extracts of PAH-rich PM strongly activated metabolizing enzymes. However, discrepancies between ROS production and AhR-related gene or enzyme induction have been noted in some studies.

For example, Lai et al. (2021) observed substantial ROS production and cell death upon exposure to PAH-rich PM, accompanied by induction of inflammatory genes (*IL-6* and *IL-8*), yet no significant activation of phase I PAH-metabolizing genes such as *CYP1A1* and *CYP1B1*. The authors suggested that detoxification enzymes regulated by the Nrf2 pathway may suppress or balance phase I gene expression, even in the presence of oxidative stress and cellular damage. Compared to EROD activity, only HS-HFO PM significantly induced BROD activity, suggesting that unique chemical compounds abundant in HS-HFO but less so in other fuel PMs are involved. Furthermore, the suppression of IL-8 release observed with HS-HFO_{SYN} PM, alongside the significant mutation frequency, supports the hypothesis of disrupted metabolizing pathways. This disruption could affect cellular processes, such as the cytoskeleton integrity and protein trafficking. These findings are consistent with the observations of Longhin et al. (2018), who showed that cytoskeletal disruption and impaired trafficking of signaling molecules, such as vesicles carrying IL-8 to the plasma membrane, can suppress the release of pro-inflammatory factors. Together, these observations emphasize the potential for disrupted metabolizing pathways to drive unexpected biological responses associated with PAH-rich PM. The results of this study indicate that simply reducing the sulfur content of marine fuels alone will not necessarily mitigate the cytotoxic, genotoxic, and mutagenic potential of these emissions. A more comprehensive evaluation of the physical and chemical properties of marine fuels is required. This study underscores the need for emission assessments to go beyond sulfur reduction in order to gain a broader understanding of the environmental and health impacts of marine fuel emissions.

5. Conclusions

This study provides a detailed analysis of the physical and chemical characteristics of PMs derived from ship emissions of different marine fuel types. The results indicate that factors beyond Sulfur content play a significant role in shaping emission profiles and influencing toxicological potentials. The marine fuels studied, including MGO and HFO with different FSC, produced distinct particle emission profiles. For instance, HFO-derived PM exhibited a predominance of smaller particle sizes compared to MGO-derived PM. In addition to differences in particle size, the chemical composition of PM varied considerably across fuel types. HFO-derived PM, in particular, contained significantly higher concentrations of PAHs, including HMW-PAHs such as Benzo[a]pyrene and Benzo[b]fluoranthene. Fuels with elevated PAH content were more effective in inducing toxicological responses, such as cytotoxicity, genotoxicity, and mutagenicity, compared to distillate fuels like MGO. These toxicological responses were not solely determined by FSC, but were strongly influenced by intrinsic PM characteristics such as PAH content and particle size. It is important to note that the biological responses induced by PM in our experiments were based on the same mass of PM, as this study focused on the quality of combustion particles in relation to fuel type and their environmental and health effects. Therefore, when interpreting the toxicological impacts of PM, it is crucial to consider the generally higher particle number and mass emission factors associated with HFOs compared to MGO, which may otherwise lead to an overestimation of the toxicological effects of MGO PM. However, the significant induction of intracellular ROS and DNA damage by MGO PM emphasizes the need for further reduction of PM emissions from all fuel types, regardless of FSC compliance.

While our study demonstrated significant biological responses, future research incorporating direct aerosol exposure at the air–liquid interface may offer a more accurate representation of real-world exposure scenarios. This approach could also enhance cell-particle interactions compared to submerged conditions and account for the role of emissions' gas-phase components. Overall, this study advances our understanding of the toxicological effects of PM emitted by ships using approved marine fuel types with regulated FSC. It underscores the importance of considering both the physical and chemical properties of marine fuels and their associated emissions when revising relevant regulations. Consequently, we advocate for the implementation of stricter legislation and additional restrictions on ship emissions, alongside the adoption of abatement systems, to mitigate the environmental and human health impacts of marine fuel emissions.

CRediT authorship contribution statement

Seongho Jeong: Writing – review & editing, Writing – original draft, Visualization, Validation, Methodology, Investigation, Formal analysis, Data curation, Conceptualization. **Jana Pantzke:** Writing – review & editing, Validation, Investigation, Formal analysis, Data curation. **Svenja Offer:** Writing – review & editing, Validation, Investigation, Formal analysis, Data curation. **Uwe Käfer:** Writing – review & editing, Validation, Investigation, Formal analysis, Data curation. **Jan Bendl:** Investigation. **Mohammad Saraji-Bozorgzad:** Investigation. **Anja Huber:** Investigation. **Bernhard Michalke:** Investigation. **Uwe Etzien:** Investigation. **Gert Jakobi:** Validation, Investigation. **Jürgen Orasche:** Investigation. **Hendryk Czech:** Writing – review & editing, Investigation, Formal analysis. **Christopher P. Rüger:** Writing – review & editing, Investigation, Formal analysis. **Jürgen Schnelle-Kreis:** Writing – review & editing, Writing – original draft, Validation, Methodology. **Thorsten Streibel:** Writing – review & editing, Resources, Project administration, Conceptualization. **Bert Buchholz:** Resources, Project administration, Funding acquisition. **Thomas Adam:** Resources, Project administration, Funding acquisition. **Martin Sklorz:** Writing – review & editing, Writing – original draft, Validation, Supervision, Methodology, Investigation, Formal analysis, Data curation, Conceptualization. **Sebastiano Di Bucchianico:** Writing – review & editing, Writing – original draft, Visualization, Validation, Supervision, Resources, Project administration, Methodology, Investigation, Funding acquisition, Formal analysis, Data curation, Conceptualization. **Ralf Zimmermann:** Writing – review & editing, Supervision, Resources, Project administration, Funding acquisition, Conceptualization.

Declaration of competing interest

The authors declare that they have no known competing financial interests or personal relationships that could have appeared to influence the work reported in this paper.

Acknowledgement

We thank the University of Rostock and Bundeswehr University for supporting this project. We also thank Ms. Verena Häfner and Dr. Tobias Stöger (ILBD/CPC, Helmholtz Munich) for the active support regarding the physical characterization of particle suspensions. We gratefully acknowledge the Analytik Service AG (ASG) for the SIMDIS measurements and support. This work was supported by the German Federal Ministry for Economic Affairs and Climate Action by the project SAARUS [grant number 03SX483D] and the dtec.bw-Digitalization and Technology Research Center of the Bundeswehr (projects "LUKAS" and "MORE"). dtec.bw is funded by the European Union – NextGenerationEU. This work was also funded by the Helmholtz Association of German Research Centers (Helmholtz International Laboratory aeroHEALTH [grant number InterLabs-0005] and the European Union's Horizon 2020 research and innovation program [grant number 955390, ULTRHAS (Ultrafine particles from TRansportation-Health Assessment of Sources)].

Appendix A. Supplementary data

Supplementary data to this article can be found online at https://doi.org/10.1016/j.envint.2025.109440.

Data availability

Data will be made available on request.

References

Åkerlund, E., Cappellini, F., Di Bucchianico, S., Islam, S., Skoglund, S., Derr, R., Odnevall Wallinder, I., Hendriks, G., Karlsson, H.L., 2018. Genotoxic and mutagenic properties of Ni and NiO nanoparticles investigated by comet assay, γ-H2AX staining, Hprt mutation assay and ToxTracker reporter cell lines. Environ. Mol. Mutagen. 59, 211–222. https://doi.org/10.1002/em.22163.

Akhtar, U.S., Rastogi, N., McWhinney, R.D., Urch, B., Chow, C.-W., Evans, G.J., Scott, J. A., 2014. The combined effects of physicochemical properties of size-fractionated ambient particulate matter on *in vitro* toxicity in human A549 lung epithelial cells. Toxicol. Rep. 1, 145–156. https://doi.org/10.1016/j.toxrep.2014.05.002.

Aksoyoglu, S., Baltensperger, U., Prévôt, A.S.H., 2016. Contribution of ship emissions to the concentration and deposition of air pollutants in Europe. Atmospheric Chem. Phys. 16, 1895–1906. https://doi.org/10.5194/acp-16-1895-2016.

Anders, L., Schade, J., Rosewig, E.I., Schmidt, M., Irsig, R., Jeong, S., Käfer, U., Gröger, T., Bendl, J., Saraji-Bozorgzad, M.R., Adam, T., Etzien, U., Czech, H., Buchholz, B., Streibel, T., Passig, J., Zimmermann, R., 2024. Polycyclic aromatic hydrocarbons as fuel-dependent markers in ship engine emissions using single-particle mass spectrometry. Environ. Sci. Atmospheres 4, 708–717. https://doi.org/10.1039/D4EA00035H.

Arrieta, D.E., Ontiveros, C.C., Li, W.-W., Garcia, J.H., Denison, M.S., McDonald, J.D., Burchiel, S.W., Washburn, B.S., 2003. Aryl hydrocarbon receptor-mediated activity of particulate organic matter from the Paso del Norte airshed along the U.S.-Mexico border. Environ. Health Perspect. 111, 1299–1305.

Bauer, M., Czech, H., Anders, L., Passig, J., Etzien, U., Bendl, J., Streibel, T., Adam, T.W., Buchholz, B., Zimmermann, R., 2024. Impact of fuel sulfur regulations on carbonaceous particle emission from a marine engine. Npj Clim. Atmospheric Sci. 7, 1–8. https://doi.org/10.1038/s41612-024-00838-4.

Bendl, J., Saraji-Bozorgzad, M.R., Käfer, U., Padoan, S., Mudan, A., Etzien, U., Giocastro, B., Schade, J., Jeong, S., Kuhn, E., Sklorz, M., Grimmer, C., Streibel, T., Buchholz, B., Zimmermann, R., Adam, T., 2024. How do different marine engine fuels and wet scrubbing affect gaseous air pollutants and ozone formation potential from ship emissions? Environ. Res. 260, 119609. https://doi.org/10.1016/j.envres.2024.119609.

Billet, S., Garçon, G., Dagher, Z., Verdin, A., Ledoux, F., Cazier, F., Courcot, D., Aboukais, A., Shirali, P., 2007. Ambient particulate matter (PM2.5): Physicochemical characterization and metabolic activation of the organic fraction in human lung epithelial cells (A549). Environ. Res. 105, 212–223. https://doi.org/10.1016/j.envres.2007.03.001.

Bonetta, Sa., Gianotti, V., Bonetta, S.i., Gosetti, F., Oddone, M., Gennaro, M.C., Carraro, E., 2009. DNA damage in A549 cells exposed to different extracts of PM2.5 from industrial, urban and highway sites. Chemosphere 77, 1030–1034. https://doi.org/10.1016/j.chemosphere.2009.07.076.

Burke, M.D., Thompson, S., Elcombe, C.R., Halpert, J., Haaparanta, T., Mayer, R.T., 1985. Ethoxy-, pentoxy- and benzyloxyphenoxazones and homologues: a series of substrates to distinguish between different induced cytochromes P-450. Biochem. Pharmacol. 34, 3337–3345. https://doi.org/10.1016/0006-2952(85)90355-7.

Cao, X., Padoan, S., Binder, S., Bauer, S., Orasche, J., Rus, C.-M., Mudan, A., Huber, A., Kuhn, E., Oeder, S., Lintelmann, J., Adam, T., Di Bucchianico, S., Zimmermann, R., 2022. A comparative study of persistent DNA oxidation and chromosomal instability induced in vitro by oxidizers and reference airborne particles. Mutat. Res. Genet. Toxicol. Environ. Mutagen. 874–875, 503446. https://doi.org/10.1016/j.mrgentox.2022.503446.

Celo, V., Dabek-Zlotorzynska, E., McCurdy, M., 2015. Chemical Characterization of Exhaust Emissions from Selected Canadian Marine Vessels: The Case of Trace Metals and Lanthanoids. Environ. Sci. Technol. 49, 5220–5226. https://doi.org/10.1021/acs.est.5b00127.

Cho, E., Allemang, A., Audebert, M., Chauhan, V., Dertinger, S., Hendriks, G., Luijten, M., Marchetti, F., Minocherhomji, S., Pfuhler, S., Roberts, D.J., Trenz, K., Yauk, C.L., 2022. AOP report: Development of an adverse outcome pathway for oxidative DNA damage leading to mutations and chromosomal aberrations. Environ. Mol. Mutagen. 63, 118–134. https://doi.org/10.1002/em.22479.

Cipoli, Y.A., Furst, L., Feliciano, M., Alves, C., 2023. Respiratory deposition dose of PM2.5 and PM10 during night and day periods at an urban environment. Air Qual. Atmosphere Health 16, 2269–2283. https://doi.org/10.1007/s11869-023-01405-1.

Corbett, J.J., Winebrake, J.J., Green, E.H., Kasibhatla, P., Eyring, V., Lauer, A., 2007. Mortality from Ship Emissions: A Global Assessment. Environ. Sci. Technol. 41, 8512–8518. https://doi.org/10.1021/es071686z.

Corbin, J.C., Mensah, A.A., Pieber, S.M., Orasche, J., Michalke, B., Zanatta, M., Czech, H., Massabò, D., Buatier de Mongeot, F., Mennucci, C., El Haddad, I., Kumar, N.K., Stengel, B., Huang, Y., Zimmermann, R., Prévôt, A.S.H., Gysel, M., 2018. Trace Metals in Soot and PM2.5 from Heavy-Fuel-Oil Combustion in a Marine Engine. Environ. Sci. Technol. 52, 6714–6722. https://doi.org/10.1021/acs.est.8b01764.

Czech, H., Stengel, B., Adam, T., Sklorz, M., Streibel, T., Zimmermann, R., 2017. A chemometric investigation of aromatic emission profiles from a marine engine in comparison with residential wood combustion and road traffic: Implications for source apportionment inside and outside sulphur emission control areas. Atmos. Environ. 167, 212–222. https://doi.org/10.1016/j.atmosenv.2017.08.022.

Di Bucchianico, S., Cappellini, F., Le Bihanic, F., Zhang, Y., Dreij, K., Karlsson, H.L., 2017. Genotoxicity of TiO2 nanoparticles assessed by mini-gel comet assay and micronucleus scoring with flow cytometry. Mutagenesis 32, 127–137. https://doi.org/10.1093/mutage/gew030.

dos Santos, T., Varela, J., Lynch, I., Salvati, A., Dawson, K.A., 2011. Quantitative Assessment of the Comparative Nanoparticle-Uptake Efficiency of a Range of Cell Lines. Small 7, 3341–3349. https://doi.org/10.1002/smll.201101076.

Durant, J.L., Busby, W.F., Lafleur, A.L., Penman, B.W., Crespi, C.L., 1996. Human cell mutagenicity of oxygenated, nitrated and unsubstituted polycyclic aromatic hydrocarbons associated with urban aerosols. Mutat. Res. Toxicol. 371, 123–157. https://doi.org/10.1016/S0165-1218(96)90103-2.

Eyring, V., Köhler, H.W., Lauer, A., Lemper, B., 2005. Emissions from international shipping: 2. Impact of future technologies on scenarios until 2050. J. Geophys. Res. Atmospheres 110. https://doi.org/10.1029/2004JD005620.

Franken, N.A.P., Rodermond, H.M., Stap, J., Haveman, J., van Bree, C., 2006. Clonogenic assay of cells in vitro. Nat. Protoc. 1, 2315–2319. https://doi.org/10.1038/nprot.2006.339.

Fresta, C.G., Chakraborty, A., Wijesinghe, M.B., Amorini, A.M., Lazzarino, G., Lazzarino, G., Tavazzi, B., Lunte, S.M., Caraci, F., Dhar, P., Caruso, G., 2018. Non-toxic engineered carbon nanodiamond concentrations induce oxidative/nitrosative stress, imbalance of energy metabolism, and mitochondrial dysfunction in microglial and alveolar basal epithelial cells. Cell Death Dis. 9, 1–13. https://doi.org/10.1038/s41419-018-0280-z.

Fritt-Rasmussen, J., Wegeberg, S., Gustavson, K., Sørheim, K.R., Daling, P.S., Jørgensen, K., Tonteri, O., Holst-Andersen, J.P., 2018. Heavy Fuel Oil (HFO) : A review of fate and behaviour of HFO spills in cold seawater, including biodegradation, environmental effects and oil spill response. Nordisk Ministerråd.

Fuglestvedt, J., Berntsen, T., Eyring, V., Isaksen, I., Lee, D.S., Sausen, R., 2009. Shipping Emissions: From Cooling to Warming of Climate—and Reducing Impacts on Health. Environ. Sci. Technol. 43, 9057–9062. https://doi.org/10.1021/es901944r.

Galluzzi, L., Vitale, I., Abrams, J.M., Alnemri, E.S., Baehrecke, E.H., Blagosklonny, M.V., Dawson, T.M., Dawson, V.L., El-Deiry, W.S., Fulda, S., Gottlieb, E., Green, D.R., Hengartner, M.O., Kepp, O., Knight, R.A., Kumar, S., Lipton, S.A., Lu, X., Madeo, F., Malorni, W., Mehlen, P., Nuñez, G., Peter, M.E., Piacentini, M., Rubinsztein, D.C., Shi, Y., Simon, H.-U., Vandenabeele, P., White, E., Yuan, J., Zhivotovsky, B., Melino, G., Kroemer, G., 2012. Molecular definitions of cell death subroutines: recommendations of the Nomenclature Committee on Cell Death 2012. Cell Death Differ. 19, 107–120. https://doi.org/10.1038/cdd.2011.96.

Genies, C., Maître, A., Lefèbvre, E., Jullien, A., Chopard-Lallier, M., Douki, T., 2013. The Extreme Variety of Genotoxic Response to Benzo[a]pyrene in Three Different Human Cell Lines from Three Different Organs. PLoS ONE 8, e78356. https://doi.org/10.1371/journal.pone.0078356.

Grigonyte, J., Nuutinen, I., Koponen, T., Lamberg, H., Tissari, J., Jokiniemi, J., Sippula, O., 2014. Evaluation of a Heat Exchanger Designed for Efficient Fine Particle Precipitation in Small-Scale Wood Combustion. Energy Fuels 28, 6058–6065. https://doi.org/10.1021/ef500958x.

Gualtieri, M., Longhin, E., Mattioli, M., Mantecca, P., Tinaglia, V., Mangano, E., Proverbio, M.C., Bestetti, G., Camatini, M., Battaglia, C., 2012. Gene expression profiling of A549 cells exposed to Milan PM2.5. Toxicol. Lett. 209, 136–145. https://doi.org/10.1016/j.toxlet.2011.11.015.

Guéguen, Y., Bontemps, A., Ebrahimian, T.G., 2018. Adaptive responses to low doses of radiation or chemicals: their cellular and molecular mechanisms. Cell. Mol. Life Sci. CMLS 76, 1255–1273. https://doi.org/10.1007/s00018-018-2987-5.

Hagemeyer, C.E., Bürck, C., Schwab, R., Knoth, R., Meyer, R.P., 2010. 7-Benzyloxyresorufin-O-dealkylase activity as a marker for measuring cytochrome P450 CYP3A induction in mouse liver. Anal. Biochem. 398, 104–111. https://doi.org/10.1016/j.ab.2009.11.004.

Halamoda-Kenzaoui, B., Ceridono, M., Urbán, P., Bogni, A., Ponti, J., Gioria, S., Kinsner-Ovaskainen, A., 2017. The agglomeration state of nanoparticles can influence the mechanism of their cellular internalisation. J. Nanobiotechnology 15, 48. https://doi.org/10.1186/s12951-017-0281-6.

Heinrich, P., Diehl, U., Förster, F., Braunbeck, T., 2014. Improving the in vitro ethoxyresorufin-O-deethylase (EROD) assay with RTL-W1 by metabolic normalization and use of β-naphthoflavone as the reference substance. Comp. Biochem. Physiol. Toxicol. Pharmacol. CBP 164, 27–34. https://doi.org/10.1016/j.cbpc.2014.04.005.

Hinds, W.C., 2011. Physical and chemical processes in aerosol systems, in: Kulkarni P., Baron, P.A., Klaus Willeke (Eds.), Aerosol Measurement: Principles, Techniques, and Applications. Wiley, pp. 31–40.

Hong, W.-J., Dong, W.-J., Zhao, T.-T., Zheng, J.-Z., Lu, Z.-G., Ye, C., 2023. Ambient PM2.5-bound polycyclic aromatic hydrocarbons in Ningbo Harbor, eastern China: seasonal variation, source apportionment, and cancer risk assessment. Air Qual. Atmosphere Health 16, 1809–1821. https://doi.org/10.1007/s11869-023-01373-6.

Hsieh, P.Y., Abel, K.R., Bruno, T.J., 2013. Analysis of Marine Diesel Fuel with the Advanced Distillation Curve Method. Energy Fuels 27, 804–810. https://doi.org/10.1021/ef3020525.

Hsu, G.W., Huang, X., Luneva, N.P., Geacintov, N.E., Beese, L.S., 2005. Structure of a High Fidelity DNA Polymerase Bound to a Benzo[a]pyrene Adduct That Blocks Replication *. J. Biol. Chem. 280, 3764–3770. https://doi.org/10.1074/jbc.M411276200.

Huang, C., Hu, Q., Wang, H., Qiao, L., Jing, S., Wang, H., Zhou, M., Zhu, S., Ma, Y., Lou, S., Li, L., Tao, S., Li, Y., Lou, D., 2018. Emission factors of particulate and gaseous compounds from a large cargo vessel operated under real-world conditions. Environ. Pollut. Barking Essex 1987 (242), 667–674. https://doi.org/10.1016/j.envpol.2018.07.036.

IMO, 2008. Report of the Marine Environment Protection Committee on its Fifty-Eighth Session MEPC 58/23.
Jang, E., Choi, S., Yoo, E., Hyun, S., An, J., 2023. Impact of shipping emissions regulation on urban aerosol composition changes revealed by receptor and numerical modelling. Npj Clim. Atmospheric Sci. 6, 1–13. https://doi.org/10.1038/s41612-023-00364-9.
Jeong, S., Bendl, J., Saraji-Bozorgzad, M., Käfer, U., Etzien, U., Schade, J., Bauer, M., Jakobi, G., Orasche, J., Fisch, K., Cwierz, P.P., Rüger, C.P., Czech, H., Karg, E., Heyen, G., Krausnick, M., Geissler, A., Geipel, C., Streibel, T., Schnelle-Kreis, J., Sklorz, M., Schulz-Bull, D.E., Buchholz, B., Adam, T., Zimmermann, R., 2023. Aerosol emissions from a marine diesel engine running on different fuels and effects of exhaust gas cleaning measures. Environ. Pollut. 316, 120526. https://doi.org/10.1016/j.envpol.2022.120526.
Käfer, U., Gröger, T., Rohbogner, C.J., Struckmeier, D., Saraji-Bozorgzad, M.R., Wilharm, T., Zimmermann, R., 2019. Detailed Chemical Characterization of Bunker Fuels by High-Resolution Time-of-Flight Mass Spectrometry Hyphenated to GC × GC and Thermal Analysis. Energy Fuels 33, 10745–10755. https://doi.org/10.1021/acs.energyfuels.9b02626.
Kendall, M., Hodges, N.J., Whitwell, H., Tyrrell, J., Cangul, H., 2015. Nanoparticle growth and surface chemistry changes in cell-conditioned culture medium. Philos. Trans. r. Soc. B Biol. Sci. 370, 20140100. https://doi.org/10.1098/rstb.2014.0100.
Kim, J.Y., Lee, S.K., Kim, C.H., Jeon, T.W., Moon, C.K., Lee, H.-S., Yoo, S.D., Lee, E.S., Jeong, T.C., 2003. Effects of polycyclic aromatic hydrocarbons on liver and lung cytochrome P450s in mice. Arch. Pharm. Res. 26, 394–404. https://doi.org/10.1007/BF02976697.
Koch, B.P., Dittmar, T., 2016. From mass to structure: an aromaticity index for high-resolution mass data of natural organic matter. Rapid Commun. Mass Spectrom. 30, 250. https://doi.org/10.1002/rcm.7433.
Kuittinen, N., Jalkanen, J.-P., Alanen, J., Ntziachristos, L., Hannuniemi, H., Johansson, L., Karjalainen, P., Saukko, E., Isotalo, M., Aakko-Saksa, P., Lehtoranta, K., Keskinen, J., Simonen, P., Saarikoski, S., Asmi, E., Laurila, T., Hillamo, R., Mylläri, F., Lihavainen, H., Timonen, H., Rönkkö, T., 2021. Shipping Remains a Globally Significant Source of Anthropogenic PN Emissions Even after 2020 Sulfur Regulation. Environ. Sci. Technol. 55, 129–138. https://doi.org/10.1021/acs.est.0c03627.
Lai, A., Baumgartner, J., Schauer, J.J., Rudich, Y., Pardo, M., 2021. Cytotoxicity and chemical composition of women's personal PM2.5 exposures from rural China. Environ. Sci. Atmospheres 1, 359–371. https://doi.org/10.1039/D1EA00022E.
Låg, M., Øvrevik, J., Refsnes, M., Holme, J.A., 2020 Nov 13. Potential role of polycyclic aromatic hydrocarbons in air pollution-induced non-malignant respiratory diseases. Respir Res. 21 (1), 299. https://doi.org/10.1186/s12931-020-01563-1.
Lehtoranta, K., Aakko-Saksa, P., Murtonen, T., Vesala, H., Ntziachristos, L., Rönkkö, T., Karjalainen, P., Kuittinen, N., Timonen, H., 2019. Particulate Mass and Nonvolatile Particle Number Emissions from Marine Engines Using Low-Sulfur Fuels, Natural Gas, or Scrubbers. Environ. Sci. Technol. 53, 3315–3322. https://doi.org/10.1021/acs.est.8b05555.
Longhin, E., Holme, J.A., Gualtieri, M., Camatini, M., Øvrevik, J., 2018. Milan winter fine particulate matter (wPM2.5) induces IL-6 and IL-8 synthesis in human bronchial BEAS-2B cells, but specifically impairs IL-8 release. Toxicol. Vitro Int. J. Publ. Assoc. BIBRA 52, 365–373. https://doi.org/10.1016/j.tiv.2018.07.016.
Lunde Hermansson, A., Hassellöv, I.-M., Moldanová, J., Ytreberg, E., 2021. Comparing emissions of polyaromatic hydrocarbons and metals from marine fuels and scrubbers. Transp. Res. Part Transp. Environ. 97, 102912. https://doi.org/10.1016/j.trd.2021.102912.
Moldanová, J., Fridell, E., Winnes, H., Holmin-Fridell, S., Boman, J., Jedynska, A., Tishkova, V., Demirdjian, B., Joulie, S., Bladt, H., Ivleva, N.P., Niessner, R., 2013. Physical and chemical characterisation of PM emissions from two ships operating in European Emission Control Areas. Atmospheric Meas. Tech. 6, 3577–3596. https://doi.org/10.5194/amt-6-3577-2013.
Mueller, L., Jakobi, G., Czech, H., Stengel, B., Orasche, J., Arteaga-Salas, J.M., Karg, E., Elsasser, M., Sippula, O., Streibel, T., Slowik, J.G., Prevot, A.S.H., Jokiniemi, J., Rabe, R., Harndorf, H., Michalke, B., Schnelle-Kreis, J., Zimmermann, R., 2015. Characteristics and temporal evolution of particulate emissions from a ship diesel engine. Appl. Energy 155, 204–217. https://doi.org/10.1016/j.apenergy.2015.05.115.
Munoz, B., Albores, A., 2011. DNA Damage Caused by Polycyclic Aromatic Hydrocarbons: Mechanisms and Markers, in: Chen, C. (Ed.), Selected Topics in DNA Repair. InTech, Rijeka, pp. 125–144. doi: 10.5772/22527.
Oecd 476,, 2016. Test No. 476: In Vitro Mammalian Cell Gene Mutation Tests using the Hprt and xprt genes. OECD.
Oeder, S., Kanashova, T., Sippula, O., Sapcariu, S.C., Streibel, T., Arteaga-Salas, J.M., Passig, J., Dilger, M., Paur, H.-R., Schlager, C., Mülhopt, S., Diabaté, S., Weiss, C., Stengel, B., Rabe, R., Harndorf, H., Torvela, T., Jokiniemi, J.K., Hirvonen, M.-R., Schmidt-Weber, C., Traidl-Hoffmann, C., BéruBé, K.A., Wlodarczyk, A.J., Prytherch, Z., Michalke, B., Krebs, T., Prévôt, A.S.H., Kelbg, M., Tiggesbäumker, J., Karg, E., Jakobi, G., Scholtes, S., Schnelle-Kreis, J., Lintelmann, J., Matuschek, G., Sklorz, M., Klingbeil, S., Orasche, J., Richthammer, P., Müller, L., Elsasser, M., Reda, A., Gröger, T., Weggler, B., Schwemer, T., Czech, H., Rüger, C.P., Abbaszade, G., Radischat, C., Hiller, K., Buters, J.T.M., Dittmar, G., Zimmermann, R., 2015. Particulate Matter from Both Heavy Fuel Oil and Diesel Fuel Shipping Emissions Show Strong Biological Effects on Human Lung Cells at Realistic and Comparable In Vitro Exposure Conditions. PLOS ONE 10, e0126536. https://doi.org/10.1371/journal.pone.0126536.
Okada, S., Kweon, C.-B., Stetter, J.C., Foster, D.E., Shafer, M.M., Christensen, C.G., Schauer, J.J., Schmidt, A.M., Silverberg, A.M., Gross, D.S., 2003. Measurement of Trace Metal Composition in Diesel Engine Participate and its Potential for Determining Oil Consumption: ICPMS (Inductively Coupled Plasma Mass Spectrometer) and ATOFMS (Aerosol Time of Flight Mass Spectrometer) Measurements. SAE Trans. 112, 338–351.
Orasche, J., Schnelle-Kreis, J., Abbaszade, G., Zimmermann, R., 2011. Technical Note: In-situ derivatization thermal desorption GC-TOFMS for direct analysis of particle-bound non-polar and polar organic species. Atmospheric Chem. Phys. 11, 8977–8993. https://doi.org/10.5194/acp-11-8977-2011.
Patashnick, H., Rupprecht, E.G., 1991. Continuous PM-10 Measurements Using the Tapered Element Oscillating Microbalance. J. Air Waste Manag. Assoc. 41, 1079–1083. https://doi.org/10.1080/10473289.1991.10466903.
Ponti, J., Kinsner-Ovaskainen, A., Norlen, H., Altmeyer, S., Andreoli, C., Bogni, A., Chevillard, S., De, A.I., Chung, S.-T., Eom, I., Fujita, K., Gilliland, D., Grollino, M.G., Gulumian, M., Hirsch, C., Ichiraku, K., Igarashi, T., Jeong, J., Jo, E., Kim, D.-Y., Kaiser, J.-P., Lagache, D., La, S.R., Lee, J.K., Lee, J., Lovera, A., Mäder-Althaus, X., Nesslany, F., Ojea, J.I., Pacchierotti, F., Pianella, F., Paget, V., Kim, T.R., Roszak, J., Rosenkranz, P., Simar, S., Stępnik, M., Vetten, M., Song, N.W., Yang, J.-Y., Rossi, F., 2014. Interlaboratory comparison study of the Colony Forming Efficiency assay for assessing cytotoxicity of nanomaterials. JRC Publ. Repos. doi: 10.2788/406937.
Quimby, B.D., Dryden, P.C., Sullivan, J.J., 1991. Selective detection of volatile nickel, vanadium, and iron porphyrins in crude oils by gas chromatography-atomic emission spectroscopy. J. High Resolut. Chromatogr. 14, 110–116. https://doi.org/10.1002/jhrc.1240140208.
Ramacher, M.O.P., Matthias, V., Aulinger, A., Quante, M., Bieser, J., Karl, M., 2020. Contributions of traffic and shipping emissions to city-scale NOx and PM2.5 exposure in Hamburg. Atmos. Environ. 237, 117674. https://doi.org/10.1016/j.atmosenv.2020.117674.
Repka, S., Erkkilä-Välimäki, A., Jonson, J.E., Posch, M., Törrönen, J., Jalkanen, J.P., 2021. Assessing the costs and environmental benefits of IMO regulations of ship-originated SOx and NOx emissions in the Baltic Sea. Ambio 50, 1718–1730. https://doi.org/10.1007/s13280-021-01500-6.
Rosewig, E.I., Schade, J., Ruser, H., Passig, J., Zimmermann, R., Adam, T.W., 2024. Detection and analysis of ship emissions using single-particle mass spectrometry: A land-based field study in the port of rostock. Germany. Atmospheric Environ. X 24, 100302. https://doi.org/10.1016/j.aeaoa.2024.100302.
Sapcariu, S.C., Kanashova, T., Dilger, M., Diabaté, S., Oeder, S., Passig, J., Radischat, C., Buters, J., Sippula, O., Streibel, T., Paur, H.-R., Schlager, C., Mülhopt, S., Stengel, B., Rabe, R., Harndorf, H., Krebs, T., Karg, E., Gröger, T., Weiss, C., Dittmar, G., Hiller, K., Zimmermann, R., 2016. Metabolic Profiling as Well as Stable Isotope Assisted Metabolic and Proteomic Analysis of RAW 264.7 Macrophages Exposed to Ship Engine Aerosol Emissions: Different Effects of Heavy Fuel Oil and Refined Diesel Fuel. PLOS ONE 11, e0157964. https://doi.org/10.1371/journal.pone.0157964.
Sarvi, A., Lyyränen, J., Jokiniemi, J., Zevenhoven, R., 2011. Particulate emissions from large-scale medium-speed diesel engines: 2. Chemical Composition. Fuel Process. Technol. 92, 2116–2122. https://doi.org/10.1016/j.fuproc.2011.06.021.
Schneider, E., Czech, H., Hansen, H.J., Jeong, S., Bendl, J., Saraji-Bozorgzad, M., Sklorz, M., Etzien, U., Buchholz, B., Streibel, T., Adam, T.W., Rüger, C.P., Zimmermann, R., 2023. Humic-like Substances (HULIS) in Ship Engine Emissions: Molecular Composition Effected by Fuel Type, Engine Mode, and Wet Scrubber Usage. Environ. Sci. Technol. 57, 13948–13958. https://doi.org/10.1021/acs.est.3c04390.
Schnelle-Kreis, J., Welthagen, W., Sklorz, M., Zimmerman, R., 2005. Application of direct thermal desorption gas chromatography and comprehensive two-dimensional gas chromatography coupled to time of flight mass spectrometry for analysis of organic compounds in ambient aerosol particles. J. Sep. Sci. 28, 1648–1657. https://doi.org/10.1002/jssc.200500120.
Shang, Y., Fan, L., Feng, J., Lv, S., Wu, M., Li, B., Zang, Y.-S., 2013. Genotoxic and inflammatory effects of organic extracts from traffic-related particulate matter in human lung epithelial A549 cells: The role of quinones. Toxicol. in Vitro 27, 922–931. https://doi.org/10.1016/j.tiv.2013.01.008.
Shimada, T., Fujii-Kuriyama, Y., 2004. Metabolic activation of polycyclic aromatic hydrocarbons to carcinogens by cytochromes P450 1A1 and 1B1. Cancer Sci. 95, 1–6. https://doi.org/10.1111/j.1349-7006.2004.tb03162.x.
Sippula, O., Stengel, B., Sklorz, M., Streibel, T., Rabe, R., Orasche, J., Lintelmann, J., Michalke, B., Abbaszade, G., Radischat, C., Gröger, T., Schnelle-Kreis, J., Harndorf, H., Zimmermann, R., 2014. Particle emissions from a marine engine: chemical composition and aromatic emission profiles under various operating conditions. Environ. Sci. Technol. 48, 11721–11729. https://doi.org/10.1021/es502484z.
Sofiev, M., Winebrake, J.J., Johansson, L., Carr, E.W., Prank, M., Soares, J., Vira, J., Kouznetsov, R., Jalkanen, J.-P., Corbett, J.J., 2018. Cleaner fuels for ships provide public health benefits with climate tradeoffs. Nat. Commun. 9, 406. https://doi.org/10.1038/s41467-017-02774-9.
Streibel, T., Schnelle-Kreis, J., Czech, H., Harndorf, H., Jakobi, G., Jokiniemi, J., Karg, E., Lintelmann, J., Matuschek, G., Michalke, B., Müller, L., Orasche, J., Passig, J., Radischat, C., Rabe, R., Reda, A., Rüger, C., Schwemer, T., Sippula, O., Stengel, B., Sklorz, M., Torvela, T., Weggler, B., Zimmermann, R., 2017. Aerosol emissions of a ship diesel engine operated with diesel fuel or heavy fuel oil. Environ. Sci. Pollut. Res. Int. 24, 10976–10991. https://doi.org/10.1007/s11356-016-6724-z.
Sueur, M., Rüger, C.P., Maillard, J.F., Lavanant, H., Zimmermann, R., Afonso, C., 2023. Selective characterization of petroporphyrins in shipping fuels and their corresponding emissions using electron-transfer matrix-assisted laser desorption/ionization Fourier transform ion cyclotron resonance mass spectrometry. Fuel 332, 126283. https://doi.org/10.1016/j.fuel.2022.126283.
Vilas-Boas, V., Chatterjee, N., Carvalho, A., Alfaro-Moreno, E., 2024. Particulate matter-induced oxidative stress – Mechanistic insights and antioxidant approaches reported

in in vitro studies. Environ. Toxicol. Pharmacol. 110, 104529. https://doi.org/10.1016/j.etap.2024.104529.
Walczyk, D., Bombelli, F.B., Monopoli, M.P., Lynch, I., Dawson, K.A., 2010. What the Cell "Sees" in Bionanoscience. J. Am. Chem. Soc. 132, 5761–5768. https://doi.org/10.1021/ja910675v.
Wang, Y., Chung, A., Paulson, S.E., 2010. The effect of metal salts on quantification of elemental and organic carbon in diesel exhaust particles using thermal-optical evolved gas analysis. Atmospheric Chem. Phys. 10, 11447–11457. https://doi.org/10.5194/acp-10-11447-2010.
Win, M.S., Tian, Z., Zhao, H., Xiao, K., Peng, J., Shang, Y., Wu, M., Xiu, G., Lu, S., Yonemochi, S., Wang, Q., 2018. Atmospheric HULIS and its ability to mediate the reactive oxygen species (ROS): A review. J. Environ. Sci. 71, 13–31. https://doi.org/10.1016/j.jes.2017.12.004.
Wu, D., Zhang, F., Lou, W., Li, D., Chen, J., 2017. Chemical characterization and toxicity assessment of fine particulate matters emitted from the combustion of petrol and diesel fuels. Sci. Total Environ. 605–606, 172–179. https://doi.org/10.1016/j.scitotenv.2017.06.058.
Wu, D., Li, Q., Ding, X., Sun, J., Li, D., Fu, H., Teich, M., Ye, X., Chen, J., 2018. Primary Particulate Matter Emitted from Heavy Fuel and Diesel Oil Combustion in a Typical Container Ship: Characteristics and Toxicity. Environ. Sci. Technol. 52, 12943–12951. https://doi.org/10.1021/acs.est.8b04471.
Yang, L., Zhang, H., Zhang, X., Xing, W., Wang, Y., Bai, P., Zhang, L., Hayakawa, K., Toriba, A., Tang, N., 2021. Exposure to Atmospheric Particulate Matter-Bound Polycyclic Aromatic Hydrocarbons and Their Health Effects: A Review. Int. J. Environ. Res. Public. Health 18, 2177. https://doi.org/10.3390/ijerph18042177.
Zerboni, A., Bengalli, R., Baeri, G., Fiandra, L., Catelani, T., Mantecca, P., 2019. Mixture Effects of Diesel Exhaust and Metal Oxide Nanoparticles in Human Lung A549 Cells. Nanomaterials 9, 1302. https://doi.org/10.3390/nano9091302.
Zetterdahl, M., Moldanová, J., Pei, X., Pathak, R.K., Demirdjian, B., 2016. Impact of the 0.1% fuel sulfur content limit in SECA on particle and gaseous emissions from marine vessels. Atmos. Environ. 145, 338–345. https://doi.org/10.1016/j.atmosenv.2016.09.022.

Glossary

AI: Aromaticity Index
BaP: Benzo[a]pyrene
BbF: Benzo[b]fluoranthene
BROD: 7-Benzyloxyresorufin-O-debenzylase
BSA: Bovine Serum Albumin
CCAI: Calculated Carbon Aromaticity Index
CFE: Colony Forming Efficiency
CYP: Cytochrome P450
DF: Dilution Factor
DMEM: Dulbecco's Modified Eagle Medium
DMSO: Dimethyl Sulfoxide
DNA: Deoxyribonucleic Acid
DTD-GC×GC-HRTOFMS: Direct Thermal Desorption comprehensive two-dimensional Gas Chromatography coupled to High-Resolution Time-Of-Flight Mass Spectrometry
eBC: Equivalent Black Carbon
EJD: Ejector Diluter
ELISA: Enzyme-Linked Immunosorbent Assay
EMS: Ethyl Methane Sulfonate
EROD: 7-Ethoxyresorufin-O-deethylase
FBS: Fetal Bovine Serum
FSC: Fuel sulfur content
HBSS: Hank's Balanced Salt Solution
HMW: High Molecular Weight
HFO: Heavy Fuel Oil
HPRT: Hypoxanthine-guanine phosphoribosyl transferase
ICP-OES: Inductively Coupled Plasma Atomic Emission Spectroscopy
IL-8: Interleukin-8
IMO: International Maritime Organization
LMW: Low Molecular Weight
MCE: Metabolic Cell Equivalent
MEF: Mutagenic Equivalency Factor
MEQ: Mutagenic Equivalent
MGO: Marine Gas Oil
PAH: Polycyclic Aromatic Hydrocarbon
PBS: Phosphate Buffered Saline
PDI: Poly Dispersity Index
PM: Particulate Matter
PTD: Porous tube diluter
ROS: Reactive Oxygen Species
SEM: Standard Error of Mean
SECA: Sulfur Emission Control Area
TE: Tris-EDTA
TG: Thioguanine